Qubit entanglement generated by classical light driving an optical cavity

Seongjin Ahn and Andrey S. Moskalenko*
Department of Physics, KAIST, Daejeon 34141, Republic of Korea

Vladimir Y. Chernyak†
Department of Chemistry, Wayne State University, 5101 Cass Avenue, Detroit, Michigan 48202, USA
and Department of Mathematics, Wayne State University, 656 West Kirby, Detroit, Michigan 48202, USA

Shaul Mukamel‡
Department of Chemistry, University of California, Irvine, California 92614, USA

(Received 17 June 2023; accepted 7 November 2023; published 4 December 2023)

We study the generation of entanglement between two qubits which communicate through a single cavity mode of quantum light but have no direct interaction. We show that such entanglement can be generated simply by exchanging quanta with a third party, which is in our case the cavity mode. Exchanging only a single quantum creates maximal entanglement. A single quantum can be provided by an external quantum light source. However, we use a classical light source to pump quanta which are used for the exchange, and investigate the degree of two-qubit entanglement. We first identify a characteristic timescale of the interaction between the cavity mode and each qubit. We investigate two regimes of the driving pulse length: one is short and the other is long compared to the characteristic timescale of the interaction. In the first regime, it is known that the pulse can pump the system by generating a displacement of the cavity mode. We show that, by using a specific pulse shape, one can make the displacement essentially vanish after the pulse finishes interaction with the cavity mode. In this case, a rotation of the qubits can be invoked. In addition, higher-order effects of the pulse including a nonlocal operation on the joint system of the cavity mode and the qubits are found, and we present a formalism to compute each term up to a given order. An explicit condition on the pulse shape for each term to be nonzero or suppressed is derived to enable an experimental design for verifying the entanglement generation using a classical light source. In the opposite regime where the driving is sufficiently long, we utilize a squeezed state which may be obtained adiabatically. We study how the squeezing and the accompanied rotation of qubits affect the generated two-qubit entanglement.

DOI: 10.1103/PhysRevResearch.5.043195

I. INTRODUCTION

If there is a direct interaction between two systems, classical light can generate entanglement between them [1–4]. However, when the two parties are not coupled, they cannot be entangled by classical light, which only allows a local unitary transformation on each party. However, quantum light can be used to create entanglement between two noninteracting systems [5–7]. Several types of quantum light have been considered to generate entanglement between qubits. In particular, the generation of entanglement between two noninteracting two-level systems (or qubits) based on cavity electrodynamics has been studied for various states of quantum light, including the Fock [8–10], thermal [11], coherent [8,12–14], and squeezed state [15,16]. The vacuum state can also be used in an off-resonant cavity to generate the qubit entanglement [17–20].

As one of the most effective and simple methods, a single-photon state of the cavity mode can be used to entangle two qubits, both resonant to the cavity mode. This can be done by exchanging a quantum, which is in this case a photon, between the cavity mode and the qubits. Suppose both qubits are in their ground states. Since there is only one photon for two qubits, only one qubit or the other, but not both at the same time, can receive the photon to get excited. Thus, the resulting state is the superposition of those two possibilities, which is an entangled state between the qubits (see also Sec. V B of Ref. [8]). Note that this is valid for a resonant cavity. Two qubits can be excited simultaneously with a single photon if the photon frequency is twice as large as that of each qubit [21]. Pumping only a single quantum directly into a cavity typically requires an external single-photon source [22,23], which is a quantum state with no classical counterpart. With

*moskalenko@kaist.ac.kr
†chernyak@chem.wayne.edu
‡smukamel@uci.edu

such a quantum light source, even a maximally entangled state can be achieved.

Then, how much entanglement can be generated if we use a classical light source for pumping the cavity mode? This is the question to investigate in this paper. We consider an exactly solvable model of two qubits interacting with a single cavity mode [24] and compute the entire time-dependent state. We explore the resulting two-qubit concurrence [25,26] as a measure for their entanglement. Previously, this has been done for several initial states of the system [8–16]. In this work, we do not assume a particular initial state other than the ground state of the total system. Instead, we drive the cavity mode with an external classical field and investigate what kind of state can be prepared. Since the cavity mode is driven by a classical light, a coherent state may be expected to a good approximation if the interaction of the cavity mode with the qubits is negligible. Some correction may be needed since the cavity mode would interact with the qubits even during the driving. We show analytically how the joint state of the cavity mode and the two qubits depends on the external classical field. The interaction between the cavity mode and the qubits is considered consistently with the external driving of the cavity mode, to identify the classes of states that can be prepared with a classical light source. We study then the entanglement generated by the prepared state. We demonstrate how the two-qubit entanglement dynamics can be controlled in terms of the strength, duration, phase, and temporal shape of the classical light field.

There are two regimes that can be distinguished in terms of the duration of the driving. Namely, it can be short or long compared to a characteristic timescale which we denote as T_g. The timescale T_g determines how fast the entanglement is generated after the system is pumped. T_g is determined by how strong the cavity mode and each qubit are coupled. When there is no coupling, no quantum can be exchanged and thus no entanglement is generated, which means $T_g \to \infty$. When there is a coupling, quanta can be exchanged and thus entanglement can be generated. The stronger the coupling is, the faster the exchange of quanta would be, which means T_g gets shorter. The precise expression of T_g is discussed. Once the characteristic timescale T_g is identified, we investigate the two mentioned driving regimes. In the regime when the cavity mode is driven by a pulse which is sufficiently short compared to T_g, we study how the two-qubit entanglement depends on the pulse strength, duration, and the shape. We show that, by selecting an appropriate pulse shape, the pumping can result in a displacement of the cavity mode or a rotation of the qubits, to a good approximation. The entanglement dynamics can be controlled by selecting the type of pumping through the pulse shape. In the latter regime, one can adiabatically generate a squeezed state and rotated qubits. The effect of the squeezing and the rotation on the entanglement formation is investigated.

This paper is organized as follows. In Sec. II, we describe the model system, where a cavity mode is driven by a classical light source. In Sec. III, we show how the entanglement can be generated by exchanging quanta between the qubits and the cavity mode. The characteristic timescale T_g of the cavity-qubit interaction is identified. In Sec. IV, we consider one of the regimes where the driving duration is sufficiently short with respect to the characteristic timescale of the cavity-qubit interaction. In Sec. V, we investigate the other regime where the driving is quasistatic. In Secs. VI and VII we discuss a set of parameters for an experimental realization and conclude the paper with a summary.

II. MODEL

We consider two qubits coupled to a resonant cavity mode of frequency ω. A classical external light drives the cavity mode. In the laboratory frame, the Hamiltonian can be written as

$$H_{\rm lab}(t) = H_f + H_g + H_{e,\rm lab}(t), \tag{1}$$

which consists of the free Hamiltonian H_f, the cavity-qubit coupling Hamiltonian H_g, and the interaction Hamiltonian $H_{e,\rm lab}(t)$ describing the coupling between the cavity mode and the classical external field. The free Hamiltonian is given by

$$H_f = \hbar\omega(a^\dagger a + \sigma^z/2).$$

Here, a and $a^\dagger$ are the annihilation and creation operators of a cavity photon, respectively. $\sigma^z = \sigma_A^z + \sigma_B^z$, with the subscript numbering the qubits. The cavity-qubit coupling term H_g can be expressed as

$$H_g = \hbar g(\sigma^+ a + \sigma^- a^\dagger). \tag{2}$$

The two-qubit ladder operator is defined as

$$\sigma^\pm = \sigma_A^\pm + \sigma_B^\pm, \tag{3}$$

where $\sigma_A^\pm$ and $\sigma_B^\pm$ are the ladder operators for qubits A and B, respectively. The interaction between the cavity mode and each qubit is described under the rotating wave approximation (RWA), which is justified for $g \ll \omega$. The last term in Eq. (1) is given by

$$H_{e,\rm lab}(t) = \hbar\Omega f(t)x,$$

where Ω is the driving strength, $f(t)$ is the temporal shape of the external field, and $x \equiv a + a^\dagger$ is the quadrature operator. In the rotating frame generated by the free Hamiltonian H_f, the model can be described by

$$H(t) = H_g + H_e(t), \tag{4}$$

where H_g remains the same as in the laboratory frame due to the cavity-qubit resonance. The second term of Eq. (4) is given by

$$H_e(t) = \hbar\Omega f(t)x_\omega(t), \tag{5}$$

where $x_\omega(t)$ is the quadrature operator in the rotating frame,

$$x_\omega(t) \equiv ae^{-i\omega t} + a^\dagger e^{i\omega t}. \tag{6}$$

The interaction Hamiltonian $H_e(t)$ describes a linearly driven oscillator, representing a cavity mode coupled to an external field. The Hamiltonian has been used theoretically [27–30] and demonstrated experimentally [31–33]. A comprehensive account for the interaction Hamiltonian can be found, e.g., in Ref. [34]. We consider a pulsed driving. Let τ_d be the duration of the pulse and $t = 0$ be the center of the pulse. The total considered time interval will be $[-T, T]$, where

$$T/\tau_d \equiv T_u \gg 1, \tag{7}$$

in order to make this time interval long enough to accommodate the pulse.

Consider a pulse with a central frequency ω which is resonant to the cavity mode and each qubit. Let $f_0(t)$ be the envelope of the pulse shape and ϕ be the carrier-envelope offset phase. We write the pulse shape as

$$f(t) = f_0(t)\cos(\omega t + \phi). \tag{8}$$

The envelope function can be expanded in a complete set of localized functions, e.g., a set of Hermite-Gaussian (HG) functions, which can be written as

$$f_{\mathrm{HG},m}(u) = N_m H_m(u) e^{-u^2/2}. \tag{9}$$

Here, $u \equiv t/\tau_d$ and $H_m(u)$ is the mth-order Hermite polynomial for $m \geqslant 0$. The normalization factor N_m is given by

$$N_m = \frac{\pi^{-1/4}}{\sqrt{m!\,2^m}},$$

so that

$$\int_{-\infty}^{\infty} du |f_{\mathrm{HG},m}(u)|^2 = 1.$$

The HG functions have a couple of suitable properties for expanding a pulse shape. First, the HG functions are orthonormal and form a complete basis set. Second, the Fourier transform of a HG function is also a HG function. This is useful for our approach since the Fourier transform of the pulse shape is used in the analytical expressions. Other complete sets of localized functions, however, may also be used to expand the pulse shape.

III. EXCHANGING QUANTA GENERATES ENTANGLEMENT

How can the two qubits become entangled? One way is to exchange a quantum with the cavity mode. For example, suppose there is no driving and consider an initial state where all the qubits are in their ground state and the cavity mode has one photon. In this case, there is only one excitation in the system, a photon. Due to the coupling between each qubit and the cavity mode, Eq. (2), the excitation starts to "move" from the cavity mode to the qubits. However, there are two qubits for a single excitation quantum. Since the coupling strength between each qubit and the cavity mode is the same, the probability that the quantum will be found after some time at one of the qubits is identical as for the other qubit. This state, where the two possibilities of a bipartite system (two qubits) are superposed, is entangled.

We will trace this entanglement generation. Let us denote the initial state $|\psi(0)\rangle$ as $|00;1\rangle \equiv |00\rangle|1\rangle$. $|00\rangle \in \mathcal{H}_q$ represents the state of two qubits where both of them are in their ground states. $|n\rangle$ with $n \geqslant 0$ denotes the Fock state with n photons in the cavity mode. $\mathcal{H}_q$ and $\mathcal{H}_\gamma$ represent the Hilbert space of the qubits and of the cavity mode, respectively. At time t, the state evolves into a certain state, denoted as $|\psi(t)\rangle$. The time evolution is governed by the Hamiltonian H_g in Eq. (2). One can diagonalize the Hamiltonian to calculate the exact expression of $|\psi(t)\rangle$. However, we note that $|\psi(t)\rangle$ would be a superposition of only two states, $|00;1\rangle$ and $|\Psi^+;0\rangle \equiv |\Psi^+\rangle|0\rangle$, where $|\Psi^+\rangle \equiv (1/\sqrt{2})(|01\rangle + |10\rangle)$. This can be seen by noting that $\sigma^+|00\rangle = \sqrt{2}|\Psi^+\rangle$ and that H_g consists of two terms, $\sigma^+ a$ and $\sigma^- a^\dagger$, which describe exchanges of quanta between both qubits and the cavity mode. Considering a time evolution with a finite time t as a succession of infinitesimal steps Δt, each approximated as $1 + (-i/\hbar)H_g \Delta t$, all possible paths that a state may evolve along can be indicated by the following diagram:

$$0 \underset{\sigma^- a^\dagger}{\longleftarrow} |00\rangle|1\rangle \underset{\sigma^- a^\dagger}{\overset{\sigma^+ a}{\rightleftharpoons}} |\Psi^+\rangle|0\rangle \xrightarrow{\sigma^+ a} 0. \tag{10}$$

From this diagram, one can expect that the state will be a superposition of the two states. An exact calculation shows that

$$U_g(t)|00;1\rangle = \cos(g_1 t)|00;1\rangle + \sin(g_1 t)|\Psi^+;0\rangle, \tag{11}$$

where $U_g(t) = \exp[-\frac{i}{\hbar}H_g t]$ and $g_1 = \sqrt{2}g$. At $t = 0$, the total state is $|00;1\rangle$ and the two qubits are not entangled. When $t = \pi/2g_1$, the total state becomes $|\Psi^+;0\rangle$, where the two qubits are in a maximally entangled state. Note that the timescale of the entanglement dynamics is proportional to $g_1^{-1} \sim g^{-1}$.

When there are $n \geqslant 2$ quanta, the state can have an additional component, namely, $|11;n-2\rangle \equiv |11\rangle|n-2\rangle$, which can be noticed by considering the possible paths as the following diagram:

$$0 \underset{\sigma^- a^\dagger}{\longleftarrow} |00\rangle|n\rangle \underset{\sigma^- a^\dagger}{\overset{\sigma^+ a}{\rightleftharpoons}} |\Psi^+\rangle|n-1\rangle \underset{\sigma^- a^\dagger}{\overset{\sigma^+ a}{\rightleftharpoons}} |11\rangle|n-2\rangle \xrightarrow{\sigma^+ a} 0.$$

An exact calculation shows that the timescale of the dynamics is proportional to $g_n^{-1} \sim (\sqrt{n}g)^{-1}$, where

$$g_n = \sqrt{4n-2}\,g \tag{12}$$

for $n \geqslant 1$. Here, we define a timescale, denoted as T_g, of the system containing n quanta as

$$T_g = (\sqrt{n}g)^{-1}.$$

The dynamics of observables for a state with n quanta will characteristically unfold at this timescale. We expect that the formation of entanglement takes about this amount of time when there are n quanta in the system.

To confirm the timescale of the entanglement dynamics, we quantify the entanglement of the reduced density operator ρ of the two qubits. The density operator is defined as

$$\rho(t) = \mathrm{tr}_\gamma[|\psi(t)\rangle\langle\psi(t)|], \tag{13}$$

where $|\psi(t)\rangle$ represents the state of the total system at time t and tr_γ is a partial trace with respect to the degree of freedom of the cavity mode. After tracing out the cavity mode, the qubits are in a mixed state in general. For instance, the reduced density operator for the state given as Eq. (11) is

$$\rho(t) = \cos^2(g_1 t)|00\rangle\langle 00| + \sin^2(g_1 t)|\Psi^+\rangle\langle\Psi^+|,$$

which is a mixed state for all times t, except for $t \neq m\pi/2g_1$ where m is an integer. A mixed state can be represented as a statistical ensemble of pure states with their associated probabilities. Each possible pure state in the ensemble has a well-defined entanglement, defined via the von Neumann entropy that represents the upper bound on the purification or entanglement cost, the latter being defined in terms of the

cooperative game that uses the local operations and classical communication (LOCC) protocols [35]. It has been also demonstrated [35] that the von Neumann entropy can only go down in average when nonunitary operations, such as measurements, are performed.

To quantify entanglement of mixed states of two qubits, the notion of entanglement of formation has been introduced as the minimal average von Neumann entropy of an ensemble of pure states that represents the given mixed state (the pure states do not have to be mutually orthogonal, and their number is not fixed), and the minimum is taken over all such ensembles [36]. It has been shown in Ref. [36] that the entanglement of formation defined in this way has the analogous property of decreasing upon nonunitary transformations, associated with measurements, and therefore is considered a good measure of entanglement for mixed states of two qubits.

Since the definition involves an optimization problem, the entanglement of formation is apparently hard to compute. Therefore, an important result is an explicit formula for the entanglement of formation in terms of the so-called concurrence, postulated in Ref. [25]. There, the concurrence was defined in terms of the eigenstates of a matrix acting in the Hilbert space of two qubits. This matrix is composed of the product of the density matrix of the given mixed state and its involuted counterpart, with the involution that comes from the antilinear operator acting in the Hilbert space of a single qubit that represents the time-reversal symmetry. The formula for the entanglement of formation in terms of the concurrence has been proven there, for a particular case of the density matrices with at least two zero eigenvalues. The proof was extended to a general mixed state of two qubits in Ref. [26].

The calculation of concurrence is related to a time-reversal operation. For qubits, which are pseudospins, this corresponds to a "spin flip." The concurrence is defined in terms of how similar is a state to its time-reversed, or spin-flipped, counterpart. For example, $|00\rangle\langle 00|$ is a product state. Its spin-flipped counterpart is $|11\rangle\langle 11|$. The similarity between the two states is quantified by the absolute value of their inner product, namely, $|\langle 11|00\rangle| = 0$, which is consistent with the zero entanglement of the state $|00\rangle$. If one does the same procedure for a maximally entangled state, say, $|\Psi^+\rangle\langle\Psi^+|$, one notices that its spin-flipped counterpart is the same, thus yielding the maximal similarity $|\langle\Psi^+|\Psi^+\rangle| = 1$. For a mixed state, the concurrence is defined as

$$C \equiv \max\{0, \tilde{C}\}, \tag{14}$$

which is either zero or a quantity called "naive" concurrence $\tilde{C}$. The naive concurrence is given as

$$\tilde{C} \equiv \lambda_1 - \lambda_2 - \lambda_3 - \lambda_4, \tag{15}$$

where $\lambda_1 \geqslant \lambda_2 \geqslant \lambda_3 \geqslant \lambda_4$ are square roots of the eigenvalues of $\rho\tilde{\rho}$. Here, $\tilde{\rho} \equiv \sigma_A^y \sigma_B^y \rho^* \sigma_A^y \sigma_B^y$ is a spin-flipped counterpart of ρ. The multiplication of ρ with $\tilde{\rho}$ and calculating its eigenvalues quantifies the similarity between ρ and $\tilde{\rho}$. By combining with signs in a special way as given in Eq. (15), it is known that the concurrence defined as Eq. (14) indeed is a measure of the entanglement of formation [26].

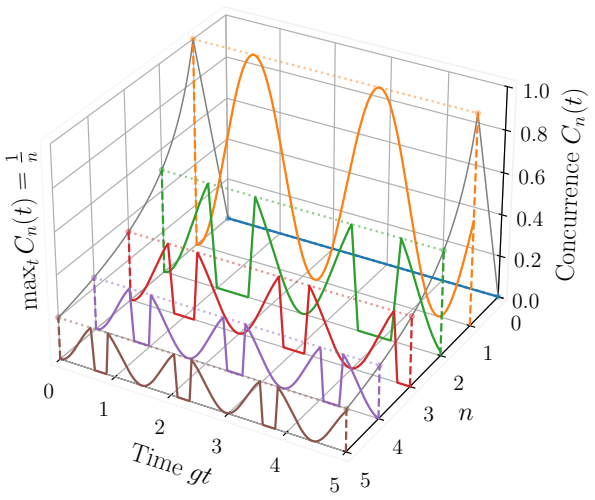

FIG. 1. The concurrence $C_n(t)$, as given by Eq. (16), when there are n photons in the initial state. The gray solid lines shown on the photon-number-concurrence planes represent the maximal concurrence, as given by Eq. (18).

We denote the concurrence as $C_n \equiv C_n(t)$ for the state $|\psi_n(t)\rangle = U_g(t)|00; n\rangle$ with $n \geqslant 0$. We get

$$C_n = \begin{cases} 0 & (n = 0) \\ \max\left\{0, \rho_n^{\Psi^+} - 2\sqrt{\rho_n^{00}\rho_n^{11}}\right\} & (n \geqslant 1), \end{cases} \tag{16}$$

where $\rho_n^\mu \equiv \rho_n^\mu(t) \equiv \langle\mu|\rho_n(t)|\mu\rangle$ is the population of a two-qubit state $|\mu\rangle$ for $\mu \in \{00, \Psi^+, 11\}$. $\rho_n(t)$ is the reduced density operator of the qubits, which is defined as Eq. (13) with $|\psi(t)\rangle = |\psi_n(t)\rangle$. The populations are given as

$$\begin{aligned} \rho_n^{00}(t) &= [p_n + q_n \cos(g_n t)]^2, \\ \rho_n^{\Psi^+}(t) &= q_n \sin^2(g_n t), \\ \rho_n^{11}(t) &= p_n q_n [1 - \cos(g_n t)]^2, \end{aligned} \tag{17}$$

where $p_n = (n-1)/(2n-1)$, $q_n = n/(2n-1)$, and g_n is defined by Eq. (12).

The maximal concurrence is achieved when there is only $n = 1$ photon in the initial state. To see this, we notice that $C_1(t) = \sin^2(g_1 t)$, which follows from Eqs. (16) and (17). Similarly, the maximal value achievable for each n can be derived as

$$\max_t C_n(t) = \begin{cases} 0 & (n = 0) \\ 1/n & (n \geqslant 1), \end{cases} \tag{18}$$

which shows that the entanglement vanishes as $n \to \infty$. This is consistent with the results in Sec. V B of Ref. [8]. In Fig. 1, we plot the concurrence $C_n(t)$ and its maximal value $\max_t C_n(t)$ for each initial photon number n. Although the photon number changes with time, the total number of quanta is conserved, which is a sum of the number of photons and the number of excited qubits. In other words, the state of the system always belongs to a subspace with n quanta. Thus, each concurrence has a well-defined period $2\pi/g_n \sim (\sqrt{n}g)^{-1} = T_g$, which determines the timescale of entanglement generation in the subspace of n quanta.

Regarding the entanglement generation mechanism, we note that what creates or eliminates the entanglement is the

set of two ladder operators, σ^+ and σ^-. On top of that, what triggers the action of these ladder operators is an event of exchanging a quantum with the cavity mode [see Eq. (10)]. Thus, when there is no quantum in the system, such as $|00\rangle|0\rangle$, no exchange of quanta can occur and no entanglement is generated.

IV. ENTANGLEMENT GENERATION BY SUBCYCLE DRIVING, $\tau_d \ll T_g$

In this section, we consider entanglement generation by a short pulse. With $\tau_d \ll T_g$, the action of the pulse on the system lasts shorter than the timescale of the interaction between the cavity and the qubits. However, we need to set also a lower bound on τ_d. First, there seems to exist a finite lower bound for the pulse duration that can be realized experimentally. Second, the pulse will possess a well-defined carrier frequency ω. This is to prevent exciting other cavity modes and to efficiently couple the external mode to the cavity mode with the desired frequency. The condition reads $\Delta\omega \ll \omega$, where $\Delta\omega$ is the bandwidth of the pulse. Combining this condition with the uncertainty relation between time and frequency, namely, $(\Delta\omega)^{-1} < \tau_d$ (or $\sim\tau_d$ for a Fourier-limited pulse), we get $\omega^{-1} \ll \tau_d$. Using both limits, one arrives at the range of pulse durations

$$g/\omega \ll g\tau_d \ll 1/\sqrt{n}. \tag{19}$$

Again, $\sqrt{n}$ is determined by the number of quanta involved in the dynamics of the state, as in Sec. III.

In this short-pulse regime, the interaction between cavity mode and the qubits would seem almost frozen during the pulse. Since only the cavity mode is externally driven, the qubits can notice the effect of the pulse only through the state of the cavity mode, which is coupled to the qubits. The higher the cavity mode–qubit coupling g, the faster can the changes in the cavity mode affect the qubits. As described in Sec. III, the interaction speed is roughly proportional to $\sqrt{n}$, where n is on the same magnitude as the number of quanta in the state undergoing the dynamics. Thus, if the pulse duration τ_d is sufficiently shorter than the interaction timescale $T_g = (\sqrt{n}g)^{-1}$, then in the leading order we can leave the qubits out of consideration while the cavity is pumped.

Formally, neglecting the cavity mode–qubit interaction translates into $g \to 0$. In this case, the total Hamiltonian in Eq. (4) reduces to $H(t) = H_e(t)$, which is a linearly driven harmonic oscillator in the rotating frame. Classically, it has an exact solution obtained by solving the Hamilton equations. In the original frame it reads

$$\begin{aligned} \dot{x}(t) &= +\omega p(t), \\ \dot{p}(t) &= -\omega x(t) - 2\Omega f(t), \end{aligned} \tag{20}$$

with the following classical-quantum correspondence: $x \leftrightarrow a + a^\dagger$, $p \leftrightarrow -ia + ia^\dagger$. Expressing the two real variables x and p by a single complex variable $z_\omega \equiv (x + ip)/2$, the Hamilton equations (20) can be combined as

$$\dot{z}_\omega(t) = -i\omega z_\omega(t) - i\Omega f(t). \tag{21}$$

In the absence of driving, i.e., $\Omega = 0$, the system exhibits a harmonic motion, $z_\omega(t) = e^{-i\omega(t-t_0)} z_\omega(t_0)$, for a given reference time point t_0. In the rotating frame defined by $z_\omega(t) \equiv e^{-i\omega t} z(t)$, the Hamilton equation for $z_\omega(t)$ given by Eq. (21) translates to

$$\dot{z}(t) = -i\Omega f(t) e^{i\omega t}.$$

The solution describes a displacement with an amplitude,

$$z(t) - z(t_0) = -i\Omega \int_{t_0}^{t} dt' f(t') e^{i\omega t'}. \tag{22}$$

Although this result comes from the classical Hamilton equations [Eqs. (20)], the same expression can be obtained from a fully quantum-mechanical description, governed by $H(t)$ in Eq. (4) with $g \to 0$. Even if g is not exactly zero, the displacement with the amplitude given in Eq. (22) is a good approximation as long as the pulse is sufficiently shorter than $(\sqrt{n}g)^{-1}$. In this approximation, the relevant number of quanta, n, at time t is around the average photon number $|z(t)|^2$. Thus, self-consistency requires

$$\tau_d \ll (\sqrt{n}g)^{-1} \sim (|z(t)|g)^{-1}$$

for all relevant times t. We may increase the amplitude z until $g\tau_d \ll 1/|z|$ still holds. In order to generate a large amplitude with a certain level of accuracy, a sufficiently short pulse is required. Exactly how small the duration should be is determined by the pulse shape. If we can understand how the accuracy depends on the pulse shape, we may be able to find a pulse shape which generates a large enough amplitude with a good fidelity, even for a moderately short pulse. In Sec. IV E, we express the fidelity as a functional of the pulse shape and utilize it to properly tailor the pulse for mitigating the error. We expect the error to come from the fact that we neglected the interaction between the qubits and the cavity. This is shown in Sec. IV C. The magnitudes of this second-order and higher-order terms are identified in the following sections. Generally, these terms occur to be smaller than the leading-order term. However, they can become essential when $z(t)$ converges to zero after the end of the pulse so that the leading-order term vanishes. We discuss the condition for such pulses with almost no displacement and generalize the idea so that one can switch on or off a term with a specific order. This can be useful since each term has its own signature. For example, the leading-order term induces a displacement of the cavity mode and the second-order term induces a rotation of the qubits.

In this section, we show that the leading-order effect of the pulse is to create a coherent state in the cavity mode. Furthermore, we formulate the conditions when this effect can be turned off by pulse shaping. Then, the second-order term becomes relevant. It acts only on the state of the qubits. We demonstrate that by shaping the pulse appropriately one can select which part of the system is pumped, either the cavity mode or the qubits. Understanding how the pulse shape controls both the amplitude of the generated coherent state and the states of the qubits is essential for an experimental realization of the entanglement generation as well as other phenomena including the collapse and revival of the qubits observables [37] and the existence of the "attractor" state [13,38].

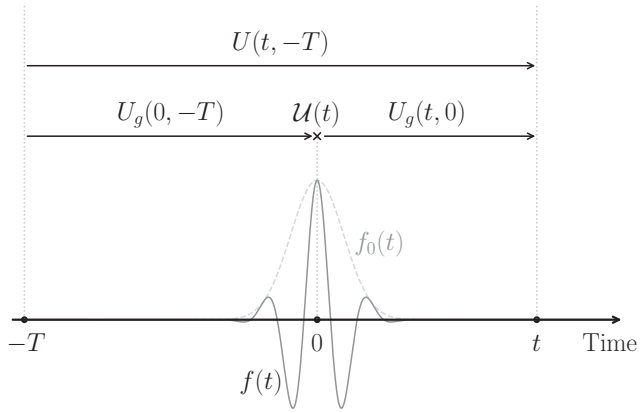

FIG. 2. The interaction picture for a pulsed driving.

A. Interaction picture for the pulse

In order to describe the effect of the pulse, we switch to a variant of the interaction picture. This is done as follows. In the absence of external driving, i.e., $\Omega = 0$, the Hamiltonian, Eq. (4), becomes time independent: $H(t) = H_g$. The time evolution from the initial time $-T$ to $t \in [-T, T]$ can be described by the total time-evolution operator

$$U(t,-T) = U_g(t,-T) = U_g(t,0)U_g(0,-T),$$

where $U(t,-T)$ and $U_g(t,t') \equiv U_g(t-t') \equiv \exp[-iH_g(t-t')/\hbar]$ are the time-evolution operators generated by $H(t)$ and H_g, respectively. In the presence of an external pulse, i.e., $\Omega > 0$, centered at time $t = 0$, we define a time-evolution operator $\mathcal{U}$:

$$U(t,-T) \equiv U_g(t,0)\mathcal{U}(t;0,-T)\,U_g(0,-T). \tag{23}$$

The time-evolution operator $\mathcal{U}$ accounts for the effect of the pulse. For brevity, we denote $\mathcal{U}(t;0,-T)$ as $\mathcal{U}(t)$. A schematic diagram of the interaction picture is shown in Fig. 2. $\mathcal{U}(t)$ satisfies

$$\dot{\mathcal{U}}(t) = -\frac{i}{\hbar}H_I(t)\mathcal{U}(t). \tag{24}$$

Here $H_I(t)$ is the Hamiltonian in the interaction picture:

$$\begin{aligned} H_I(t) &= U_g^\dagger(t)[H(t) - H_g]U_g(t) \\ &= \hbar\Omega\tilde{H}_I(t), \end{aligned} \tag{25}$$

with

$$\tilde{H}_I(t) = f(t)\,U_g^\dagger(t)\,x_\omega(t)\,U_g(t). \tag{26}$$

Since $\tilde{H}_I(t)$ is proportional to the pulse shape $f(t)$, it impacts the evolution of the system only for a short duration of time, τ_d. If the pulse is sufficiently shorter than the cavity-qubits timescale, i.e., $\tau_d \ll T_g$, then $U_g(t)$ in Eq. (26) essentially remains identity during the interaction with the pulse, so that $\tilde{H}_I(t) \simeq f(t)x_\omega(t)$. Formally, this can be seen by using the identity of Campbell [39],

$$e^X Y e^{-X} = Y + [X,Y] + \tfrac{1}{2}[X,[X,Y]] + \ldots, \tag{27}$$

to expand $\tilde{H}_I(t)$ in powers of $g\tau_d$,

$$\begin{aligned} \tilde{H}_I(u) = (g\tau_d)^0 f(u)x_\omega(u) + (g\tau_d)^1 f(u)u[i\tilde{H}_g, x_\omega(u)] \\ + \mathcal{O}[(g\tau_d)^2], \end{aligned} \tag{28}$$

where $\tilde{H}_g \equiv H_g/\hbar g$ and $u \equiv t/\tau_d$.

B. Leading-order effect: Displacement of the cavity mode

The solution of Eq. (24) can be expressed in terms of the Magnus expansion [40],

$$\mathcal{U}(t) \equiv \exp[-iA_I(t)], \tag{29a}$$

$$A_I(t) = \sum_{m=1}^{\infty} A_I^{(m)}(t). \tag{29b}$$

Each term $A_I^{(m)}(t)$ in the expansion (29b) is an m-fold integral of a product of m Hamiltonians H_I. For example, the first two terms are given as

$$A_I^{(1)}(t) = \frac{1}{\hbar}\int_{-T}^{t} dt' H_I(t'),$$

$$A_I^{(2)}(t) = -\frac{i}{2\hbar^2}\int_{-T}^{t} dt' \int_{-T}^{t'} dt'' \,[H_I(t'), H_I(t'')].$$

The expression for $A_I^{(m)}(t)$ for any $m \geqslant 2$ is given as Eq. (B3) in Appendix B. The expansion is known to absolutely converge [41,42] if $H_I(t)$ is bounded and

$$\int_{-T}^{t} dt' \left\| -\frac{i}{\hbar}H_I(t') \right\|_2 < \pi, \tag{31}$$

where $\|O\|_2 \equiv \max_{\langle\psi|\psi\rangle=1} \langle\psi|O^\dagger O|\psi\rangle^{1/2}$ denotes the 2-norm of an operator O. This is a sufficient condition for the convergence, implying that the series may still converge even if the integral in Eq. (31) exceeds π. Note that $\|U^\dagger O U\|_2 = \|O\|_2$ for any unitary operator U, i.e., the 2-norm is invariant under unitary transformations. Using this invariance and substituting $u \equiv t/\tau_d$, the convergence condition, Eq. (31), reads

$$\Omega\tau_d \int_{-T_u}^{t/\tau_d} du\, |f(u)| \|x\|_2 < \pi. \tag{32}$$

Although a and $a^\dagger$ are not bounded in the whole Fock space, they are bounded in the n-quanta subspace. As long as the state belongs to at most a composite space of one or more n-quanta subspaces, the operator $x = a + a^\dagger$ is bounded and on the order of $\sqrt{n}$, where n can be thought of as an average number of quanta in the system. Then the convergence condition, Eq. (32), reads

$$\mathcal{O}[\sqrt{n}\Omega\tau_d] < \pi, \tag{33}$$

implying that for a sufficiently small $\sqrt{n}\Omega\tau_d$, the Magnus expansion Eq. (29) would converge and thus an approximate expression can be obtained by considering the leading terms of the expansion.

The exponent $A_I(t)$ of $\mathcal{U}$ is expanded in powers of $\Omega\tau_d$ so that

$$A_I^{(m)}(t) \equiv (\Omega\tau_d)^m \tilde{A}_I^{(m)}(t) \tag{34a}$$

$$= \mathcal{O}[(\sqrt{n}\Omega\tau_d)^m] \tag{34b}$$

for each $m \geqslant 1$. For brevity, let us denote $\tilde{\Omega}_n \equiv \sqrt{n}\Omega\tau_d$. We then get

$$A_I^{(m)}(t) = \mathcal{O}[(\tilde{\Omega}_n)^m]. \tag{35}$$

The factor $\sqrt{n}$ in Eq. (34b) comes from the fact that the total degree of $\tilde{A}_I^{(m)}(t)$ is m in a and $a^\dagger$, whose matrix elements in the subspace of n quanta are on the order of $\sqrt{n}$. A derivation of Eq. (34) is presented in Appendix B. When $\tilde{\Omega}_n \equiv \sqrt{n}\Omega\tau_d \ll 1$, the leading-order term is $A_I^{(1)}(t)$, which can be written in terms of

$$\tilde{A}_I^{(1)}(t) = \int_{-T/\tau_d}^{t/\tau_d} du \tilde{H}_I(u).$$

In order to see the dominant effect of a short pulse such that $\tau_d/T_g = \sqrt{n}g\tau_d \equiv \tilde{g}_n \ll 1$, we substitute $\tilde{H}_I(u)$ with Eq. (28) and take the leading-order term in $g\tau_d$. We get then

$$\tilde{A}_I^{(1)}(t) = \tilde{A}_I^{(1,0)}(t) + \mathcal{O}(g\tau_d), \tag{36}$$

where

$$\begin{aligned}\tilde{A}_I^{(1,0)}(t) &\equiv A_I^{(1,0)}(t)/(\Omega\tau_d) \\ &= s_1(t)\, a + s_1^*(t)\, a^\dagger,\end{aligned} \tag{37}$$

with

$$s_1(t) = \int_{-T/\tau_d}^{t/\tau_d} du f(u) e^{-i\omega\tau_d u}. \tag{38}$$

After the pulse, i.e., when $t \gg \tau_d$, and with T satisfying Eq. (7), $s_1(t)$ becomes

$$s_1 \simeq \hat{f}(\omega\tau_d), \tag{39}$$

where $\hat{f}(k) \equiv \int_{-\infty}^{\infty} du f(u) e^{-iku}$ is the Fourier transform of $f(u)$. By controlling the central frequency component of the pulse, one can make $s(t)$ either zero or nonzero for $t \gg \tau_d$.

In our case, the pulse consists of a central frequency ω and an envelope $f_0(t)$ with the carrier-envelope phase ϕ, as written in Eq. (8). Thus, the Fourier component of $f(u)$ at $\omega\tau_d$ can be expressed as

$$\hat{f}(\omega\tau_d) = \tfrac{1}{2} e^{i\phi} \hat{f}_0(0) + \tfrac{1}{2} e^{-i\phi} \hat{f}_0(2\omega\tau_d), \tag{40}$$

where $\hat{f}_0(k)$ is the Fourier transform of the envelope function $f_0(u)$. Note that $f_0(u)$ is defined in the scaled time domain $u \equiv t/\tau_d$, with duration $\tau_d/\tau_d = 1$. Thus, the width of $\hat{f}_0(k)$ in the Fourier domain is also on the order of 1. If one considers a pulse with a well-defined carrier frequency, we get $\omega\tau_d \gg 1$, in line with Eq. (19). In this regime, $\hat{f}_0(2\omega\tau_d)$ in Eq. (40) almost vanishes, so that the functional s_1 can be approximated as

$$s_1 \simeq \tfrac{1}{2} e^{i\phi} \hat{f}_0(0). \tag{41}$$

From Eqs. (29), (34), and (36), we get the leading-order term of $\mathcal{U}$,

$$\begin{aligned}\mathcal{U}(t) &= \exp[-iA_I(t)] && \text{(42a)}\\ &\simeq \exp[-iA_I^{(1)}(t)] && \text{(42b)}\\ &\simeq \exp[-iA_I^{(1,0)}(t)] && \text{(42c)}\\ &\equiv U_1(t), && \text{(42d)}\end{aligned}$$

where the second line holds for $\sqrt{n}\Omega\tau_d \ll 1$ and the third line for $\sqrt{n}g\tau_d \ll 1$. The $U_1(t)$ denotes the leading-order term. From Eq. (37), one can show that the leading term U_1 is a displacement operator,

$$U_1(t) = D[z(t)],$$

where the complex amplitude of the displacement can be written as

$$z(t) = -i\Omega\tau_d s_1^*(t). \tag{43}$$

The phase, or direction, of the displacement can be controlled by the carrier-envelope offset phase ϕ, as can be seen from Eq. (41).

If $z(t) \simeq 0$ after the pulse, i.e., $t \gg \tau_d$, the leading-order term U_1 has only a transient modulation during the pulse. In order to drive the cavity mode into a coherent state with a nonzero amplitude z after the pulse, a pulse with $s_1(t) \neq 0$ for $t \gg \tau_d$ is required. With the asymptotic expression for s_1 given by Eq. (41), this requires an envelope $f_0(t)$ such that $\hat{f}_0(0) = \int_{-\infty}^{\infty} dt\, f_0(t) \neq 0$. For example, a Gaussian shape $f_{\mathrm{HG},0}(t)$ can be used. The concurrence induced by a subcycle pulse with such a shape is shown in Fig. 3.

Depending on the pulse area $\Omega\tau_d$, characteristics of the time-dependent concurrence vary. For example, for a small pulse area, i.e., $\Omega\tau_d \ll 1$, the average number of quanta pumped into the cavity, which is given by $|z(T)|^2$, is much smaller than one. Thus, the concurrence is dominated by the interference between states belonging to few-quanta subspaces. This can be seen in Fig. 3(a). When $\Omega\tau_d \sim 1$ such that the generated coherent state has an average photon number of around one, i.e., $|z|^2 \sim 1$, a value of concurrence larger than 0.75 can be achieved, which is shown in Fig. 3(b). This is consistent with the case of a Fock state where the single-photon state allows to achieve maximal entanglement. When many photons are pumped into the cavity mode, so that $|z|^2 \gg 1$, a smooth oscillation of concurrence appears, as shown in Fig. 3(c). This is consistent with the concurrence generated by a strong coherent state [13,14].

We note that the driving strengths Ω used in Figs. 3(b) and 3(c) may not be small enough to satisfy the convergence condition, Eq. (33) for the Magnus expansion in Eq. (29b). Still, the analytical results shown in Figs. 3(b) and 3(c), which are based only on the leading term in $g\tau_d$ of the first term of the Magnus expansion, determined by Eqs. (37) and (42d) and corresponding to the so-called impulsive approximation [43], seem to agree well with the numerical results. In the following section, we account for the agreement by two steps. First, we observe that if we work in a "deeper" interaction picture generated by U_1, the corresponding Magnus expansion converges for the parameters used in Fig. 3. Second, we derive the expression for the next-order term from which we find that the pulse shape in Fig. 3(d) actually makes this term vanish after the pulse, accounting for the demonstrated accuracy of the approximation based on U_1.

C. The second-order effect: Rotation of the qubits

The propagator $U_1(t)$ is a good approximation of $\mathcal{U}(t)$ when $\sqrt{n}\Omega\tau_d \ll 1$ and $\sqrt{n}g\tau_d \ll 1$. Thus, even if the pulse is short, satisfying the latter condition, if the pulse area $\sqrt{n}\Omega\tau_d$

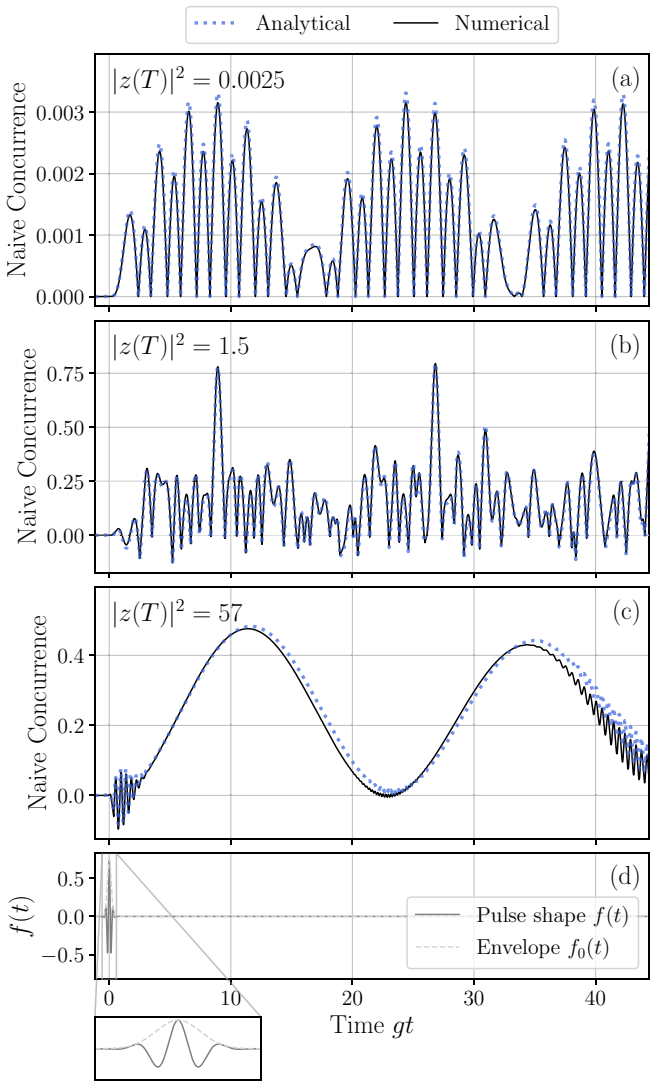

FIG. 3. Naive concurrence induced by a subcycle pulse with different driving strengths Ω, given by (a) $\Omega\tau_d = 0.0531$, (b) $\Omega\tau_d = 1.29$, and (c) $\Omega\tau_d = 8$. The pulse duration, envelope, carrier-envelope phase, and the cavity-qubit coupling are fixed as $\tau_d = \pi/\omega$, $f_0(t) = f_{\mathrm{HG},0}(t)$, $\phi = 0$, and $g = 0.05\omega$, respectively. The black solid lines (blue dotted lines) represent numerically (analytically) evaluated naive concurrences. The analytical results are obtained essentially by approximating the time-evolution operator by a displacement operator, i.e., $\mathcal{U}(t) \simeq D[z(t)]$ based on Eq. (42). The displacement amplitude $z(t)$ is given by Eq. (43). (a)–(c) The corresponding average photon numbers $|z(t)|^2$ at the end of the pulse $t = T$ are indicated in each panel. (d) The gray solid line and the light gray dashed line show the pulse shape $f(t)$ and its envelope $f_0(t)$, respectively.

is not small enough, $U_1(t)$ may not be sufficient to describe the dynamics. This is because the series in Eq. (29b) may diverge for a large $\sqrt{n}\Omega\tau_d$, in which even the inclusion of high-order terms may not work.

In order to describe the case where $\sqrt{n}\Omega\tau_d$ is not too small, we generalize the approach of Ref. [43], where the following decomposition of $\mathcal{U}$ is used:

$$\mathcal{U}(t) \equiv U_1(t)\mathcal{U}_2(t). \tag{44}$$

In order to evaluate $\mathcal{U}_2(t)$, we find the Hamiltonian which generates $\mathcal{U}_2(t)$. Let us denote the Hamiltonian as $H_{II}(t)$. Then the time-evolution operator $\mathcal{U}_2(t)$ satisfies $\dot{\mathcal{U}}_2(t) = (-i/\hbar)H_{II}(t)\mathcal{U}_2(t)$. From Eq. (44), we get the Hamiltonian,

$$H_{II}(t) = U_1^\dagger(t)[H_I(t) - H_1(t)]U_1(t), \tag{45}$$

where $H_I(t)$ and $H_1(t)$ are the Hamiltonians generating $\mathcal{U}(t)$ and $U_1(t)$, respectively. $H_I(t)$ can be evaluated from Eqs. (25) and (26). $H_1(t)$ can be obtained by differentiating $U_1(t)$ and using the definition of $H_1(t)$, namely, $\dot{U}_1(t) = (-i/\hbar)H_1(t)U_1(t)$. The derivative of $U_1(t)$ can be obtained by using the Zassenhaus formula [40] or

$$\frac{d}{dt}e^{A(t)} = \int_0^1 ds\, e^{sA(t)}\frac{dA}{dt}e^{-sA(t)}e^{A(t)},$$

which is shown in, e.g., Ref. [44]. We can then get the Hamiltonian $H_1(t)$ as

$$H_1(t) = H_e(t) - \tfrac{1}{2}\langle z(t)|H_e(t)|z(t)\rangle, \tag{46}$$

where $|z(t)\rangle \equiv D[z(t)]|0\rangle$ is a coherent state with the amplitude $z(t)$ given as Eq. (43). Inserting Eqs. (25) and (46) into the expression for $H_{II}(t)$ in Eq. (45), we get

$$H_{II}(t) = H'_{II}(t) + H_{II,z}(t),$$

where

$$H'_{II}(t) \equiv U_1^\dagger(t)[U_g^\dagger(t)H_e(t)U_g(t) - H_e(t)]U_1(t), \tag{47a}$$

$$H_{II,z}(t) \equiv \tfrac{1}{2}\langle z(t)|H_e(t)|z(t)\rangle. \tag{47b}$$

Since $H_{II,z}(t)$ is a scalar, it can be subtracted from $H_{II}(t)$ by the transformation

$$\mathcal{U}_2 \equiv U_{II,z}(t)\mathcal{U}'_2(t), \tag{48}$$

with

$$U_{II,z}(t) = \exp\left[-\frac{i}{\hbar}\int_{-T}^{t} dt' H_{II,z}(t')\right].$$

We get then the differential equation

$$\dot{\mathcal{U}}'_2(t) = -\frac{i}{\hbar}H'_{II}(t)\mathcal{U}'_2(t),$$

whose formal solution is again given by the Magnus expansion,

$$\mathcal{U}'_2(t) \equiv \exp[-iA'_{II}(t)], \tag{49a}$$

$$A'_{II}(t) = \sum_{m=1}^{\infty} A'^{(m)}_{II}(t). \tag{49b}$$

However, the order of magnitude of each term is different from that of $A_I^{(m)}(t)$ in Eq. (29b). In Appendix B, we show that

$$A'^{(m)}_{II}(t) = \mathcal{O}[(\tilde{\Omega}_n\tilde{g}_n)^m]. \tag{50}$$

It has an additional factor, $\tilde{g}_n \equiv \sqrt{n}g\tau_d$, compared to the previous case, $A_I^{(m)}(t) = \mathcal{O}[(\tilde{\Omega}_n)^m]$ in Eq. (35). This arises from a property of $H'_{II}(t)$, given by Eq. (47a), where $H_e(t)$ is subtracted from $U_g^\dagger(t)H_e(t)U_g(t)$. Applying the identity (27)

to $U_g^\dagger(t)H_e(t)U_g(t)$, the Hamiltonian can be expanded as

$$\begin{aligned}\tilde{H}'_{II}(u) &\equiv H'_{II}(u)/\hbar\Omega \\ &= (g\tau_d)^1 f(u)uU_1^\dagger(u)[i\tilde{H}_g, x_\omega(u)]U_1(u) + \mathcal{O}[(g\tau_d)^2].\end{aligned} \tag{51}$$

We note that $\tilde{H}'_{II}(t) = \mathcal{O}[(g\tau_d)^1]$, whereas $\tilde{H}_I(t) = \mathcal{O}[(g\tau_d)^0]$, as can be seen from Eq. (28).

For $\tilde{\Omega}_n\tilde{g}_n \ll 1$, the dominant term in the expansion (49b) is $A'^{(1)}_{II}(t)$ [cf. Eq. (50)]. This condition allows us to use a pulse such that $1 < \tilde{\Omega}_n \ll (\tilde{g}_n)^{-1}$ by using a sufficiently short pulse $\tilde{g}_n \ll 1$. Note that if we use the Magnus expansion in Eq. (29b) to get the second- and higher-order terms, the pulse area has to be limited by $\tilde{\Omega}_n \ll 1$ to ensure the expansion convergence. By shifting to the second interaction picture, Eq. (48), we can use a pulse with a larger $\tilde{\Omega}_n$. This is required to generate a coherent state with amplitude much larger than 1 since $z(t) = \mathcal{O}[\Omega\tau_d]$. Phenomena such as the collapse and revival of qubits observables are visible only in this regime [37].

Using Eq. (51) to evaluate $A'^{(1)}_{II}(t)$, we get

$$A'^{(1)}_{II}(t) = A'^{(1,1)}_{II}(t) + \mathcal{O}\big[\tilde{\Omega}_n\tilde{g}_n^2\big]. \tag{52}$$

The leading term is given as

$$\begin{aligned}\tilde{A}'^{(1,1)}_{II}(t) &\equiv A'^{(1,1)}_{II}(t)/(\Omega\tau_d)(g\tau_d) \\ &= s_{(1,1)}(t)(-i\sigma^-) + s^*_{(1,1)}(t)(i\sigma^+),\end{aligned} \tag{53}$$

where

$$s_{(1,1)}(t) = \int_{-T/\tau_d}^{t/\tau_d} du\, u f(u) e^{-i\omega\tau_d u}.$$

Similar to s_1 in Eq. (39), when $t \gg \tau_d$, $s_{(1,1)}(t)$ can be approximated as

$$s_{(1,1)} \simeq i\hat{f}^{(1)}(\omega\tau_d),$$

where $\hat{f}^{(1)} \equiv d\hat{f}/dk$ is the derivative of the Fourier transform $\hat{f}$ of f. In our case, the pulse has a well-defined carrier frequency ω, entering Eq. (8), which means $\omega\tau_d \gg 1$. Therefore, the functional can be approximated as

$$s_{(1,1)} \simeq \tfrac{1}{2}e^{i\phi} i\hat{f}_0^{(1)}(0), \tag{54}$$

where $\hat{f}_0^{(1)} \equiv d\hat{f}_0/dk$. Note that for any envelope $f_0(u)$ with even parity, $\hat{f}_0^{(1)}(0) = 0$.

From Eqs. (49), (50), and (52), we now get the second leading-order term as

$$\begin{aligned}\mathcal{U}'_2(t) &= \exp[-iA'_{II}(t)] && (55a)\\ &\simeq \exp[-iA'^{(1)}_{II}(t)] && (55b)\\ &\simeq \exp[-iA'^{(1,1)}_{II}(t)] && (55c)\\ &\equiv U_2(t), && (55d)\end{aligned}$$

where the second line holds for $\tilde{\Omega}_n\tilde{g}_n \ll 1$ and the third line for $\tilde{g}_n \ll 1$. The last line defines the second-leading term $U_2(t)$. With Eq. (53), one can show that $U_2(t)$ is a rotational operator:

$$U_2(t) = R[\theta(t); \mathbf{n}(t)],$$

where $R[\theta; \mathbf{n}] \equiv \exp[-i\theta\mathbf{n}\cdot\boldsymbol{\sigma}/2]$ for an angle θ, a rotational axis $\mathbf{n}$ of unit length, and $\boldsymbol{\sigma} = (\sigma^x, \sigma^y, \sigma^z)$ with $\sigma^j \equiv \sigma_A^j + \sigma_B^j$ for $j \in \{x, y, z\}$. It rotates the Bloch vector of each qubit. The angle and the rotational axis are given as

$$\theta(t) = 2(\Omega\tau_d)(g\tau_d)|s_{(1,1)}(t)|, \tag{56a}$$

$$\mathbf{n}(t) = (\sin[\phi_{(1,1)}(t)], -\cos[\phi_{(1,1)}(t)], 0), \tag{56b}$$

for $s_{(1,1)}(t) \equiv |s_{(1,1)}(t)|e^{i\phi_{(1,1)}(t)}$.

In order to have a nonzero rotation after the pulse, i.e., $\theta(t) \neq 0$ for $t \gg \tau_d$, we need a pulse envelope $f_0(t)$ with $s_{(1,1)}(t) \neq 0$ for $t \gg \tau_d$, as follows from Eq. (56). Using Eq. (54), the condition reads $i\hat{f}_0^{(1)}(0) = \int_{-\infty}^{\infty} du\, u f_0(u) \neq 0$. Thus, if the pulse envelope is even, the rotational angle essentially vanishes. If we use an odd envelope, a nonzero rotation is possible. In this case, the leading-order contribution U_1 is turned off after the pulse since $s_1(t) \simeq 0$ for $t \gg \tau_d$. This can be viewed as an instance of a catalytic process in that the cavity mode functions as a catalyst since it returns to the initial state after interacting with the pulse while inducing changes in the qubits state. This is just an opposite case of, e.g., Ref. [45], where a qubit acts as a catalyst to alter the state of the cavity mode. The concurrence induced by a subcycle pulse with an odd envelope is shown in Fig. 4. Comparing Fig. 4 with Fig. 3, the cavity-qubit coupling g, the normalized pulse duration $g\tau_d$, and the pulse area $\Omega\tau_d$ are the same in both figures. The only difference is the shape of the pulse envelope $f_0(t)$, resulting in qualitatively distinct dynamics of the concurrence.

A stronger driving results in an increased angle of rotation. An angle larger than $\pi/2$ is achieved in Fig. 4(b). There, the numerical result shows that there is an additional effect of the pulse on top of the displacement $U_1 = D[z]$ and the rotation $U_2 = R[\theta, \mathbf{n}]$. Those additional corrections can be attributed to higher-order terms which are treated in the following section.

We note that neither U_1 nor U_2 generates any entanglement, since they are local unitary transformations. Thus, for $\mathcal{U} \simeq U_1U_2$, the concurrence remains essentially zero during the interaction between the system and the driving pulse. However, both operations can pump the system to have excitations: U_1 pumps photons to the cavity mode and U_2 can excite each qubit. The entanglement builds up when the excitations pumped by the pulse are exchanged between the cavity mode and each qubit. This process is induced by the free propagation U_g, which is why the concurrence starts to grow after the pulse.

D. Higher-order effects: Conditional displacement and rotation around the z axis

The first two leading-order effects are identified as a displacement of the cavity mode and a rotation of the qubits. One may describe the effect of the pulse approximately with these two operations. However, there are higher-order terms which do not vanish in general. Understanding the higher-order terms might help to find other possible types of operations apart from the displacement or the rotation.

As an example, we present two quadratic terms in $g\tau_d$. They can be found by expanding the exponent $A'_{II}(t)$, Eq. (49b), in the orders of $\Omega\tau_d$ and $g\tau_d$. There are only two

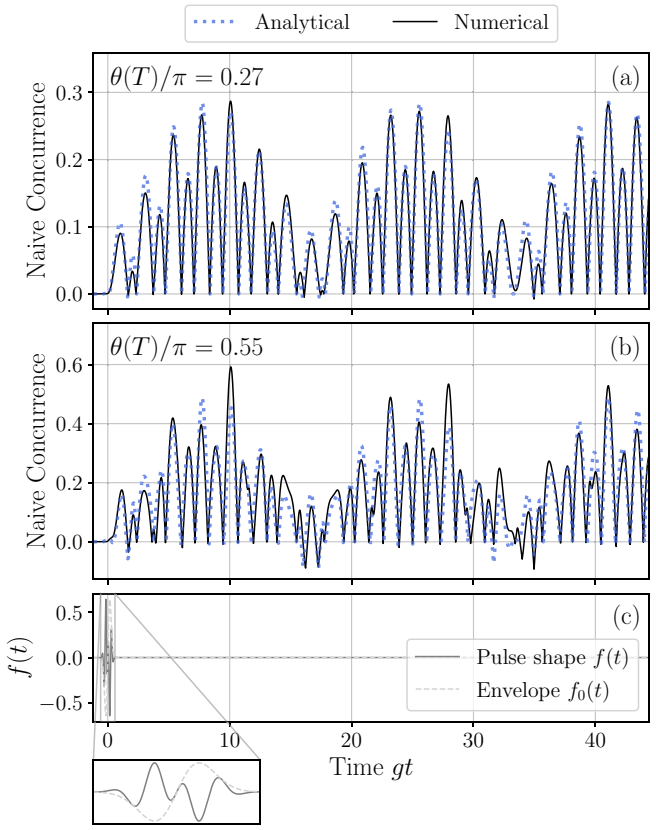

FIG. 4. Same as Fig. 3, except that the pulse envelope is given by $f_0(t) = f_{\mathrm{HG},1}(t)$ and the driving strength Ω is given by (a) $\Omega\tau_d = 2.05$ and (b) $\Omega\tau_d = 4.1$. The analytical solution is based on the approximation $\mathcal{U}(t) \simeq D[z(t)]R[\theta(t);\mathbf{n}(t)]$, i.e., including the terms up to the second order. The expressions for the displacement amplitude $z(t)$, the rotational angle $\theta(t)$, and the rotational axis $\mathbf{n}(t)$ are given by Eqs. (43), (56a), and (56b), respectively. For the given envelope, the displacement amplitude almost vanishes after the pulse, i.e., at $t = T$. The rotational angle at the end of the pulse, $\theta(T)$, is indicated in (a) and (b).

such terms, $A_{II}^{\prime(1,2)}(t)$ and $A_{II}^{\prime(2,2)}(t)$, which are quadratic in $g\tau_d$. The first term $A_{II}^{\prime(1,2)}(t)$ generates a conditional displacement where the direction to which the cavity mode is displaced depends on the state of the qubits. To be explicit,

$$\tilde{A}_{II}^{\prime(1,2)}(t) \equiv A_{II}^{\prime(1,2)}(t)/(\Omega\tau_d)(g\tau_d)^2 = \sigma^z[s_{(1,2)}(t)a + s_{(1,2)}^*(t)a^\dagger].$$

The functional $s_{(1,2)}(t)$ modulates the displacement amplitude and is given as

$$s_{(1,2)}(t) = \int_{-T/\tau_d}^{t/\tau_d} du \frac{u^2}{2!} f(u) e^{-i\omega\tau_d u}.$$

The second term $A_{II}^{\prime(2,2)}(t)$ represents a rotation of qubits around the z axis:

$$\tilde{A}_{II}^{\prime(2,2)}(t) \equiv A_{II}^{\prime(2,2)}(t)/(\Omega\tau_d)^2(g\tau_d)^2 = \sigma^z[s_{(2,2)}(t) + s_{(2,2)}^*(t)].$$

The functional $s_{(2,2)}(t)$ determines the corresponding angle of rotation and can be written as

$$s_{(2,2)}(t) = s_{(2,2),1}(t) + s_{(2,2),2}(t),$$

where

$$s_{(2,2),1}(t) = \int_{-T/\tau_d}^{t/\tau_d} du \frac{u^2}{2!} f(u)(-i)s_1^*(u)e^{-i\omega\tau_d u},$$

$$s_{(2,2),2}(t) = \int_{-T/\tau_d}^{t/\tau_d} du \frac{u}{1!} f(u)(-i)s_{(1,1)}^*(u)e^{-i\omega\tau_d u},$$

originate from the first and the second Magnus terms generated by $H_{II}^{\prime}(t)$, Eq. (49b), respectively.

E. Towards exact operation

Another advantage of identifying the higher-order terms is improvement of the accuracy of a given operation. One can enhance the accuracy of an operation by eliminating irrelevant terms. This can be done by searching a set of the driving parameters, including the pulse shape, which makes those terms vanish.

As an example, let us discuss how to obtain a displacement with a given amplitude z_0 with a certain accuracy. From the displacement amplitude $z(t)$ given by Eq. (43) we require that at the end of the operation, $t = T$, the amplitude of the displacement reaches the desired value z_0, i.e., $z(T) = z_0$. One can indeed find parameters satisfying this requirement. For $T \gg \tau_d$ and $\omega\tau_d \gg 1$, being valid in the considered regime, we can use Eq. (41). By selecting a pulse shape such that $\hat{f}(0) > 0$, we obtain

$$\Omega\tau_d \simeq 2|z_0|/\hat{f}_0(0), \tag{57a}$$

$$\phi \simeq -\phi_0 - \pi/2, \tag{57b}$$

where $z_0 \equiv |z_0|e^{i\phi_0}$.

The error in the resulting operation with respect to the displacement determined by Eq. (57a) can be estimated in terms of the normalized pulse duration $g\tau_d$. One can show that as $g\tau_d \to 0$ the error becomes arbitrarily small. In practice, the pulse cannot be infinitesimally short but has a finite duration. For a given finite pulse duration, what is important is the order of the error in terms of $g\tau_d$. In order to quantify the error, we use the state fidelity, comparing the target state with the actual state. Starting from the ground state $|\psi(-T)\rangle = |00;0\rangle$ of the system at time $t = -T$, the pulse finishes displacing the cavity mode by $z(T) = z_0$ at time $t = T$. In the interaction picture defined by Eq. (23), the target state, denoted as $|\psi_0\rangle = |00;z_0\rangle \equiv |00\rangle|z_0\rangle$, is a displaced ground state, where $|z_0\rangle \equiv D[z_0]|0\rangle$ is a coherent state. The state fidelity F is defined as the probability of measuring the target state from the actual state of the system $|\psi(T)\rangle \equiv \mathcal{U}(T)|\psi(-T)\rangle$:

$$F = |\langle\psi_0|\psi(T)\rangle|^2.$$

Using Eq. (44) with Eq. (48) and identifying $U_1(T) = D[z(T)] = D[z_0]$, the fidelity can be written as

$$F = |\langle 00;0|\mathcal{U}_2'(T)|00;0\rangle|^2. \tag{58}$$

The leading-order term, which is the displacement, cancels out the displacement of the target state and what is left is $\mathcal{U}_2'(T)$. Thus, the dominant error term for the displacement

operation is determined by the leading term of $\mathcal{U}_2'(T)$, which is $A_{II}'^{(1,1)}(T)$. For a fixed $\Omega\tau_d$ as given in Eq. (57a), the order of magnitude of the error term is

$$A_{II}'^{(1,1)}(T) = \mathcal{O}[(g\tau_d)].$$

Note that $A_{II}'^{(1,1)}(T)$ is the only term that is linear in $g\tau_d$ in the exponent $A_{II}'(T)$ of $\mathcal{U}_2'(T)$. Let us denote $A_{II}'^{(:,1)}(T) = A_{II}'^{(1,1)}(T)$, where ":" in the superscript implies "all" orders of $\Omega\tau_d$ for the given order of $g\tau_d$ which is 1 in this case. Expanding $\mathcal{U}_2'(T)$ with respect to $g\tau_d$, we arrive at

$$F = 1 - (g\tau_d)^2 \mathrm{Var}\big[\tilde{A}_{II}'^{(:,1)}(T)\big] + \mathcal{O}[(g\tau_d)^3],$$

where $\tilde{A}_{II}'^{(:,1)}(t) \equiv A_{II}'^{(:,1)}(t)/(g\tau_d) = \tilde{A}_{II}'^{(1,1)}(t)$ and the variance is evaluated with respect to the initial state $|\psi(-T)\rangle = |00;0\rangle$. In general, especially for a pulse envelope without definite parity, $\tilde{A}_{II}'^{(1,1)}(T)$ is nonzero, as can be seen from Eq. (53). An example of such a pulse envelope is $f_0(t) = (1/\sqrt{2})f_{\mathrm{HG},0}(t) + (1/\sqrt{2})f_{\mathrm{HG},1}(t)$. However, when the pulse envelope has an even parity, e.g., $f_0(t) = f_{\mathrm{HG},0}(t)$, then the leading error term, $\tilde{A}_{II}'^{(1,1)}(T)$, almost vanishes, which can be seen from Eqs. (53) and (54). Since the linear term in $g\tau_d$ is almost zero, the error is dominated by quadratic terms. As shown in Sec. IV D, there are two quadratic terms in $g\tau_d$. Denoting their sum as

$$\begin{aligned} A_{II}'^{(:,2)}(t) &= A_{II}'^{(1,2)}(t) + A_{II}'^{(2,2)}(t) \\ &\equiv (g\tau_d)^2 \tilde{A}_{II}'^{(:,2)}(t), \end{aligned}$$

the fidelity can be written as

$$F = 1 - (g\tau_d)^4 \mathrm{Var}\big[\tilde{A}_{II}'^{(:,2)}(T)\big] + \mathcal{O}[(g\tau_d)^5].$$

In Fig. 5, we show the fidelity for $z_0 = -0.05i$ and for two exemplary shapes of the pulse envelope $f_0(t)$. For both pulse shapes, the error converges to zero as the pulse duration becomes shorter. For $f_0(t) = f_{\mathrm{HG},0}(t)$ the convergence rate is higher. In this case the leading term $A_{II}'^{(1,1)}(T)$ of the error is suppressed since the functional $s_{(1,1)}(T)$ in Eq. (53) almost vanishes. A higher convergence rate implies that for a given requirement on the fidelity a longer pulse can be utilized. This is more desirable for experimental realization, because too short pulses can be problematic both in terms the generation and avoiding certain types of operation errors, as mentioned in the beginning of this section. One may go beyond the presented convergence rate by eliminating even higher-order error terms $A_{II}'^{(:,k)}(T)$ for $k \geqslant 2$, through the pulse shaping. By this method, one may systematically increase the convergence rate to the extent that a desired operation with a required fidelity can be implemented based on a pulse of available duration.

V. ENTANGLEMENT GENERATION BY QUASISTATIC DRIVING, $\tau_d \gg T_g$

We consider a quasistatic driving where the duration τ_d of the external driving is longer than the characteristic timescale of the system, T_g. We first assume that the envelope function is constant, i.e., $f_0(t) = 1$. For a fixed driving amplitude Ω, we describe the ground state of the Hamiltonian. Then, we increase the driving strength adiabatically from zero to a finite

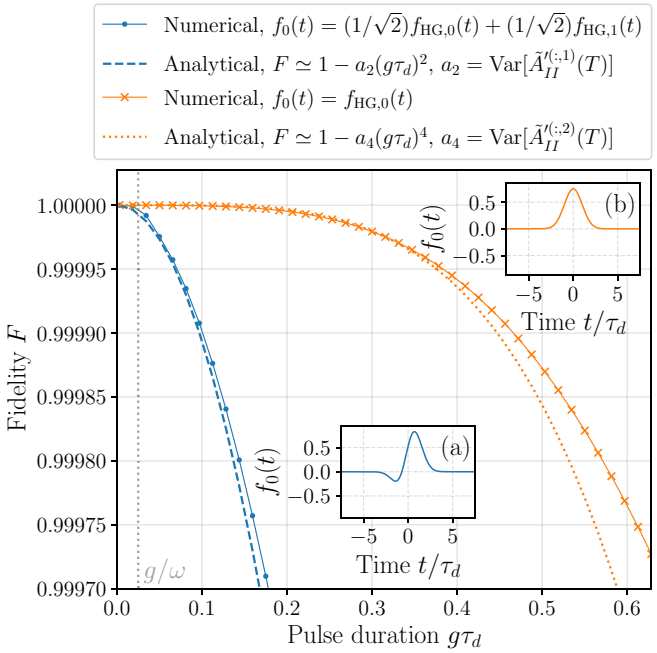

FIG. 5. State fidelity for a displacement operation $D[z_0]$ with $z_0 = -0.05i$, implemented by a subcycle pulse. The blue solid line with circles (blue dashed line) indicates numerically (analytically) evaluated fidelity for an envelope shown in inset (a). Likewise, the orange solid line with crosses (orange dotted line) represents numerically (analytically) evaluated fidelity for an envelope shown in inset (b).

value, so that the system remains in the ground state corresponding to the instantaneous value of the driving strength at each time moment.

For this quasistatic driving, we set $\phi = 0$ and $f_0(t) = 1$ in Eq. (8). Notice that, under RWA, a nonzero ϕ would correspond to a rotation of both the state of the cavity mode in its phase space and the state of the qubits, by the same angle ϕ. Thus, we have $f(t) = \cos(\omega t) = (1/2)(e^{-i\omega t} + e^{i\omega t})$. Using this in Eq. (5) and applying the RWA, we get

$$H_e^{\mathrm{RWA}} = \hbar\Omega\tfrac{1}{2}(a + a^\dagger).$$

Note that for the RWA to hold, the driving strength Ω should be small enough with respect to the driving frequency ω. The total Hamiltonian given in Eq. (4) becomes time independent:

$$H^{\mathrm{RWA}} = H_g + H_e^{\mathrm{RWA}}. \tag{59}$$

The ground state of H^{RWA} is known for an arbitrary number of qubits [46]. It is normalizable when $\Omega < Ng$, where N is the number of qubits. Let us denote the state vector corresponding to the ground state as $|E_0;r\rangle$ with energy E_0. One can show that the ground state is given by a product state of the rotated qubits and a squeezed state of the cavity mode, with the ground-state energy $E_0 = 0$. For our two-qubit case ($N = 2$), it can be written as

$$|E_0;r\rangle = |\theta_r\theta_r\rangle|r\rangle,$$

where

$$|\theta_r\theta_r\rangle \equiv R[\theta_r;\mathbf{e}_y]|00\rangle \tag{60}$$

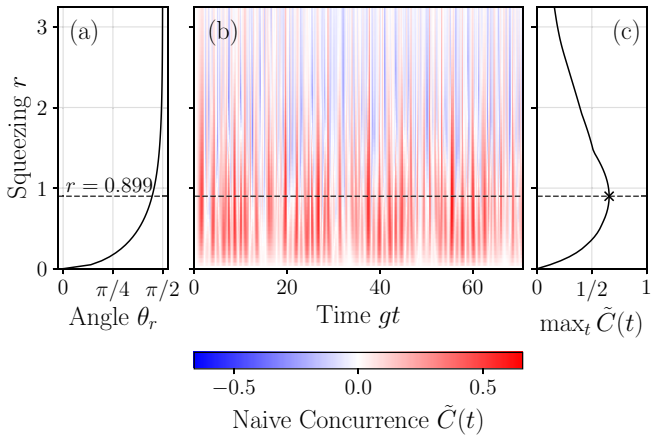

FIG. 6. (a) The relation between the squeezing parameter r of the cavity mode and the rotational angle θ_r for the qubits. (b) The naive concurrence $\tilde{C}(t)$ versus the squeezing parameter r and time t. (c) Naive concurrence maximized with respect to time for each given squeezing r.

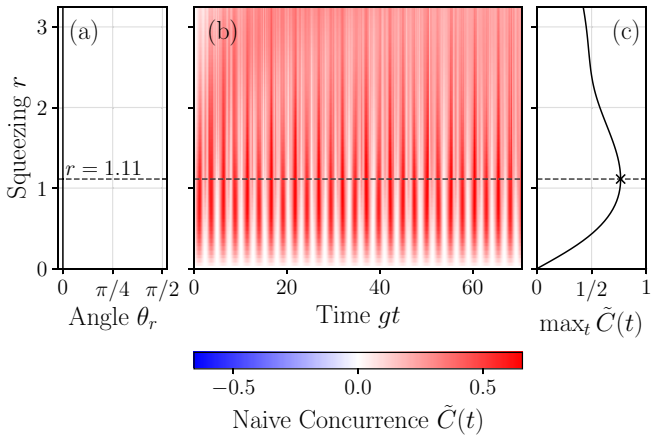

FIG. 7. Same as Fig. 6, except that the rotational angle is zero for all values of the squeezing parameter r.

and $R[\theta_r; \mathbf{e}_y]$ rotates the qubits by an angle θ_r around the y axis. The angle depends on the driving strength Ω, as determined by the relation

$$\sin\theta_r = \frac{\Omega}{Ng} = \frac{\Omega}{2g},$$

where $0 \leqslant \theta < \pi/2$ for $\Omega < Ng = 2g$. The cavity mode is squeezed,

$$|r\rangle \equiv S(r)|0\rangle,$$

where $S(r) = \exp[(r/2)(a^\dagger)^2 - (r/2)a^2)]$ is the squeezing operator with $r \geqslant 0$ being the squeezing parameter. The average photon number of $|r\rangle$ is

$$\bar{n}_\gamma \equiv \langle a^\dagger a\rangle = \sinh^2 r.$$

The rotational angle is connected to the squeezing parameter by

$$\cos\theta_r = e^{-2r}, \tag{61}$$

where $0 \leqslant r < \infty$. Figure 6(a) illustrates the relation between r and θ_r. The average number of excited qubits is given as

$$\bar{n}_q \equiv \sum_{j=1}^{N} \langle \sigma_j^+ \sigma_j^- \rangle = N \sin^2(\theta_r/2),$$

where $N = 2$ is the number of qubits and the average is taken with respect to the rotated state, Eq. (60). The total average excitation number $\bar{n}$ is defined as the sum of the average number of photons and that of the excited qubits:

$$\bar{n} = \bar{n}_\gamma + \bar{n}_q.$$

By turning off the external driving at time $t = 0$, we mean $\Omega = 2g\sin\theta_r \to 0$ instantaneously. Then the system starts to evolve with the initial condition $|\psi(0)\rangle = |E_0; r\rangle$ and with the Hamiltonian $H(t) = H_g$ since $\Omega = 0$. The concurrence evolves accordingly for $t \geqslant 0$, which is shown in Fig. 6(b). In order to find the squeezing parameter with the maximal entanglement of formation, we evaluate the naive concurrence $\tilde{C}(t)$ maximized with respect to time, i.e., $\max_t \tilde{C}(t)$, which is shown in Fig. 6(c). The maximization is done for the time range presented in Fig. 6(b). The maximal concurrence occurs for $r = 0.899$ corresponding to the average photon number $\bar{n}_\gamma = 1.05$, average number of excited qubits $\bar{n}_q = 0.83$, and the average total excitation number $\bar{n} = 1.89$. For larger squeezing, the maximal concurrence decreases. Note that the rotational angle converges to $\pi/2$ as $r \to \infty$.

To see the pure effect of the squeezed state on the generation of entanglement, one may rotate the qubits back to their ground states while keeping the squeezing of the cavity mode. For the rotations, one may address the qubits directly, by shining a laser along a direction perpendicular to the axis of the cavity. If it is not feasible to access the qubits directly, one can still rotate them by driving the cavity mode. In order to achieve this, one may drive the cavity mode with a specific pulse shape that satisfies $z(T) = 0$, in order to avoid displacement of the cavity mode but still to induce the required rotation of the qubits, facilitated by the second-order term discussed in Sec. IV C. An example of such a pulse shape can be found in Fig. 4(c).

In Fig. 7(b), we show the naive concurrence induced purely by a squeezed state, without any rotation, i.e., $\theta_r = 0$, as shown in Fig. 7(a). We notice that the naive concurrence can be negative when the rotation is involved as can be seen in Fig. 6(b), whereas, when the rotation is subtracted out resulting in a pure squeezed state, the naive concurrence stays always nonnegative.

Another difference concerns the value of the squeezing parameter r which maximizes the concurrence. As can be seen from Fig. 7, the concurrence reaches its maximum at $r = 1.11$, which corresponds to the average photon number $\bar{n}_\gamma = 1.84$. The rotation shifts the optimal squeezing parameter r and the corresponding average photon number. Without rotation, a higher average photon number is required to get the maximal concurrence. This difference in the average photon number is compensated by the pumping of quanta through the rotation (see Fig. 8). In order to generate a maximal concurrence, what matters most is the total number of excitations in the system, including both the photons and the excitations of the qubit system.

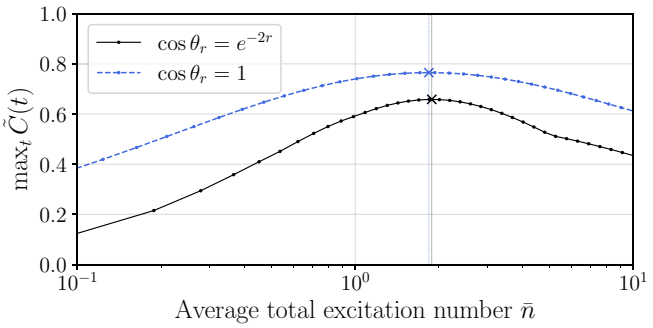

FIG. 8. Naive concurrence maximized with respect to time versus the average total excitation number. The black solid line with circles denotes the case where the rotation is accompanied by the squeezing, whereas the blue dashed line represents the case where no rotation is involved.

We finish this section by considering two limits. The first is the low-excitation limit, $\bar{n} \ll 1$. In Fig. 9(a), we show the time-dependent naive concurrence in the low-squeezing regime, where $r = 0.0492$ corresponding to $\bar{n} = 0.0962$ with rotation and $\bar{n} = 0.00243$ without rotation. We see that when there is no rotation, an oscillation with a well-defined period is present. The reason is that in this limit the initial state consists of $|00;0\rangle$ and a small amount of $|00;2\rangle$. The former has no time dependence. The latter belongs to the two-quanta subspace and is essentially the only contribution to the time dependence in this regime. When the rotation enters, however, the oscillation of the concurrence has multiple frequencies, as can be seen in Fig. 9(a), indicated by the black solid line. This can be understood as a consequence of an additional interference with another state with a single quantum, namely, $|\Psi^+;0\rangle$, introduced by the rotation of $|00;0\rangle$.

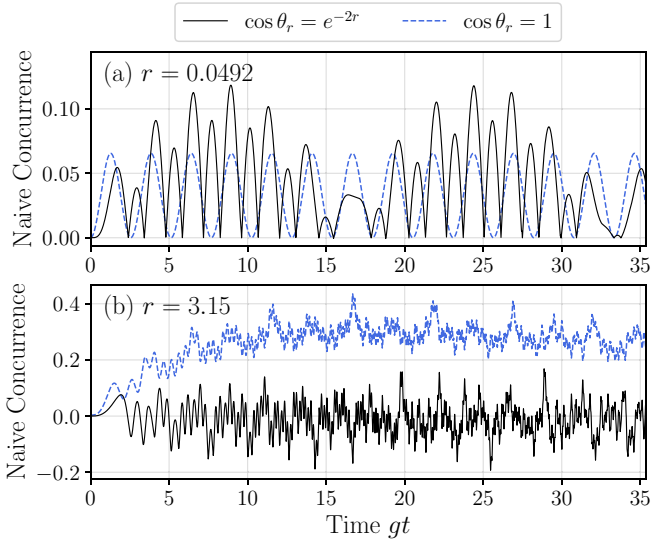

FIG. 9. Comparison of the naive concurrence with and without the rotation. The squeezing parameters are shown in each panel. The black solid lines represent the inducing of concurrence by a squeezed state with no rotation. The blue dashed lines represent the naive concurrence from a squeezed and rotated state with the rotational angle θ_r given as Eq. (61).

We next turn to the opposite regime, where the excitation number is much higher than 1. One example is shown in Fig. 9(b), where the squeezing parameter is $r = 3.15$. The corresponding average total excitation number with rotation is $\bar{n} = 137$ and that without rotation is $\bar{n} = 136$. After some time passes, the naive concurrence in both cases shows complicated fluctuations. When the rotation is not subtracted, the naive concurrence fluctuates around an average value close to zero, whereas when the initial state is purely a squeezed state with the rotation removed, the system can maintain positive entanglement of formation for longer duration.

VI. DISCUSSION

Let us discuss the relevant parameters for experimental realization of the presented results. First, since the theory employs the RWA for the coupling between each qubit and the cavity mode, the coupling strength should be small compared to the frequency of the cavity mode and the qubits, i.e., $g \ll \omega$. Second, for the subcycle, or sub-Rabi, driving, we require $g\tau_d \ll 1$, which follows from $\tau_d \ll T_g = (\sqrt{n}g)^{-1}$. For the efficient coupling of the external field to the cavity mode, without affecting much the other modes, the pulse needs to have a well-defined carrier frequency which is resonant with the frequency of the cavity mode. From this condition, we require $\omega\tau_d \gg 1$, which follows from $T_\omega \equiv 2\pi/\omega \ll \tau_d$. All the conditions can be summarized by Eq. (19). As long as the cavity-qubit coupling g, the mode frequency ω, and the pulse duration τ_d satisfy this condition, one can test the demonstrated results. To have a concrete example, we consider a quantum dot in a photonic crystal [31], where the resonant frequency corresponds to a wavelength $\lambda = 928$ nm and the cavity-qubit coupling $g/2\pi = 16$ GHz. This imposes a condition on the pulse duration as

$$T_\omega \equiv 2\pi/\omega \sim 3\ \text{fs} \ll \tau_d \ll 55\ \text{ps}/\sqrt{n} \sim 2\pi/(\sqrt{n}g).$$

For the low-excitation limit, where $n \sim 1$, we get $\tau_d \ll 55$ ps. If one selects $\tau_d = 5.5$ ps, it corresponds to $g\tau_d \sim 0.6$, which is used in our calculations, e.g., in Fig. 5. Another physical system where this model can be tested consists of superconducting qubits coupled to a common resonator. Experiments have been realized at few-qubit [32] and many-qubit [33] limits. An important issue to ensure is that the decay rate of each qubit and the cavity should be sufficiently lower than the cavity-qubit coupling g, in order to observe a coherent dynamics of concurrence on a timescale longer than T_g. A collection of experimentally realized cavity parameters including the cavity-qubit coupling strength and the decay rates for the qubits and the cavity can be found in Ref. [47].

Next, we discuss a potential multiqubit generalization of the presented results. We expect that the form of the leading-order term U_1, which is a displacement operator of the cavity mode, as well as that of the second-order term U_2, which is a rotational operator for qubits, would remain the same. The only modification of the model would be the definition of $\sigma^\pm$, from Eq. (3) to $\sum_{j=0}^{N-1} \sigma_j^\pm$, where N is the number of qubits. Thus, the subcycle pulse would be able to drive the initial ground state to a product state of a coherent state of the cavity mode and the rotated qubits, where the only difference is the total number of qubits. The reduced density

operator for a pair of qubits can be obtained by tracing out the cavity mode and the other $N-2$ qubits. The two-qubit reduced density operator would in general represent a mixed state. How the concurrence would be affected by the presence of the other qubits is a question of immediate interest that can be investigated in the near future. The two-qubit entanglement is expected to vanish as the total number of qubits in the system increases and approaches the thermodynamic limit, where the number of qubits goes to infinity. This is at least partly because the interaction in the system is nonlocal in the sense that a single cavity mode is connected to all qubits. Thus, if an entanglement between qubits is generated, its structure should be also nonlocal. Entangling only a subset of qubits is unlikely due to the qubit exchange symmetry for all involved qubits. For this reason, looking at only two qubits by tracing out the other $N-2$ qubits and the cavity mode would barely capture such nonlocal entanglement.

To understand the entanglement structure that may not be captured by the two-qubit concurrence, another entanglement measure is required. For a three-qubit pure state, there are at least two inequivalent measures which can be used to formulate a necessary and at the same time sufficient condition for the entanglement [48]. Generalizing these entanglement measures to the case of mixed states seems to be a challenging task. However, a set of efficient estimators for both the lower and the upper bound of a mixed-state entanglement has been proposed and experimentally demonstrated [49]. Other approaches to understand the multiqubit entanglement include the spectroscopic spin squeezing [50,51] and the quantum Fisher information [14,52], which provide sufficient conditions for a given state to be entangled. To study the multiqubit system in more detail, information scrambling among qubits can be studied using the tripartite mutual information [53]. The concept of *information lattice*, which is a hierarchy of local information from the smallest subsystem to that from the largest, may also be an interesting alternative way to characterize the nonlocal entanglement [54]. It is expected that the entanglement structure which is hard to capture by the two-qubit concurrence may be revealed by the information lattice.

VII. CONCLUSIONS

We have considered the generation of entanglement between two qubits by using a classical light source and a quantized cavity mode. We have shown how two qubits can be entangled by exchanging quanta with a third party which in our case is the cavity mode. Quanta can be pumped into the system through an external driving by a classical light source coupled to the cavity mode, with no direct driving of the qubits. The quanta exchange timescale $T_g = (\sqrt{n}g)^{-1}$ is identified. With respect to this characteristic timescale of the cavity-qubits system, we considered two regimes of the external driving.

We first discussed the subcycle driving, where it is performed by a pulse with duration shorter than the characteristic timescale of the system, T_g. We showed that the leading-order effect of a pulsed driving is a displacement of the cavity mode, which can be expected since the cavity mode is directly coupled to the pulse. We further showed that by shaping the pulse, one can also rotate the qubits, and if desired, one can let the cavity remain intact after the passage of the pulse. The entanglement generation for each type of the pulse shape was demonstrated, showing good agreement with exact results. We showed that the error for the displacement operation can be set arbitrarily small by choosing a sufficiently small $g\tau_d$, which represents the shortness of the pulse duration with respect to T_g. The error was estimated by identifying the convergence rate. Furthermore, enhancing the convergence rate by shaping the pulse was demonstrated, indicating how to perform a desired operation with a given fidelity. Higher-order effects including the phase shift of the qubits and the displacement of the cavity mode conditional to the qubits state are found.

As the opposite regime of the driving, we discussed a quasistatic driving where its duration is much longer than T_g. We considered a continuous-wave driving with the driving amplitude such that there exists a normalizable ground state in the rotating frame. In this regime, the ground state is a squeezed state with rotated qubits. Assuming adiabatic driving to prepare the ground state with nonzero squeezing, we studied the entanglement induced by the squeezed and rotated state. We observed a maximal entanglement of formation when the total number of excitations, which is a sum of the average photon number and the average number of excited qubits, is on the order of 1. We compared the result with the case of pure squeezing where there is no rotation of the qubits and found that the optimal value of the squeezing parameter slightly changes. However, the average total number of excitations which generates the maximal entanglement was found to remain essentially the same.

The studied cavity-qubits system is a useful testbed for fundamental quantum properties of light-matter interaction and entanglement. The presented framework enables selecting specific operations on the joint cavity-qubits state by an appropriate pulse shaping of an external classical light. The set of all possible operations accessible by the subcycle or the quasistatic driving and how each operation can be activated or suppressed with prescription for a high fidelity can be used for a laser-based experimental generation and control of the entanglement between noninteracting systems.

ACKNOWLEDGMENTS

S.A. was supported by the education and training program of the Quantum Information Research Support Center, funded through the National Research Foundation of Korea (NRF) by the Ministry of Science and ICT (MSIT) of the Korean government under Grant No. 2021M3H3A103657313. S.A. and A.S.M. were supported by the NRF grant funded by the Korean government (MSIT) under Grant No. 2020R1A2C1008500. V.Y.C. and S.M. were supported by the U.S. Department of Energy (DOE), Office of Science, Basic Energy Sciences, under Award No. DE-SC0022134. S.M. was also supported by the National Science Foundation (NSF).

APPENDIX A: VALIDITY OF THE RWA FOR A SHORT PULSE

We check the validity of the usage of the RWA in Eq. (2) on the coupling between the cavity mode and each qubit. In Fig. 10, we compare the naive concurrence obtained with

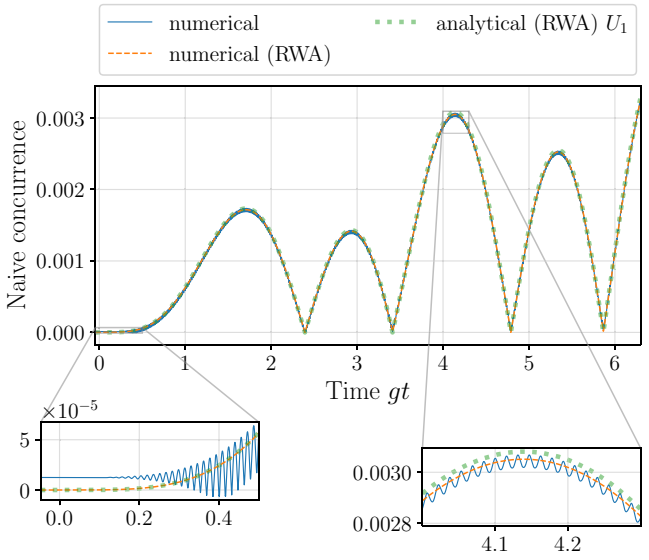

FIG. 10. The naive concurrence of the two qubits calculated with different methods. The dashed and solid lines are numerical solutions, respectively with and without the rotating wave approximation (RWA) between the cavity and each qubit. The dotted line is obtained by the analytical expression based on $\mathcal{U} \simeq U_1$. The cavity mode is driven by a pulse with duration $\tau_d = T_\omega/45$, strength $\Omega = 0.225\omega$, and shape $f(t) = \exp[-(t/\tau_d)^2]$. The coupling strength between the cavity mode and each qubit is $g = 0.005\omega$.

and without the RWA. In each calculation, their respective ground states are used. Note that the ground state under the RWA is $|00;0\rangle$ which is separable, whereas the ground state without the RWA is entangled with concurrence on the order of 10^{-5}. In the full (RWA-free) result, there is a relatively rapid oscillation on top of the longer-scale evolution, coming from the counter-rotating terms in the Hamiltonian, which are neglected under the RWA. If the amplitude of the rapid oscillation becomes comparable to the magnitude of the naive concurrence, one may not completely ignore the counter-rotating terms. In the studied cases the value of the naive concurrence is large enough with respect to the rapid oscillation, justifying the RWA. For the subcycle driving, we note that all data presented in this paper do not rely on the RWA between the cavity mode and the external field, being consistent with Eq. (5).

APPENDIX B: ORDERS OF MAGNITUDE OF MAGNUS TERMS

In this section, we derive Eqs. (34) and (50) to obtain sufficient conditions for the convergence of the Magnus expansions in Eqs. (29b) and (49b), respectively. For general discussions on the Magnus expansion, see Ref. [40].

Let us start from the first Magnus expansion, Eq. (34). The first term of the expansion can be written as

$$A_I^{(1)}(t) \equiv (\Omega\tau_d)\tilde{A}_I^{(1)}(t), \tag{B1}$$

where

$$\begin{aligned}\tilde{A}_I^{(1)}(t) &= \int_{-T/\tau_d}^{t/\tau_d} du\, \tilde{H}_I(u) \\ &= \mathcal{O}[(\Omega\tau_d)^0]\end{aligned} \tag{B2}$$

and $\tilde{H}_I(u) \equiv H_I(u)/\hbar\Omega$ is defined in Eq. (25). Any following term, i.e., $A_I^{(m)}(t)$ for $m > 1$, can be written in terms of its preceding terms, i.e., $A_I^{(k)}(t)$ for $1 \leqslant k < m$, as [41]

$$\begin{aligned}A_I^{(m)}(t) = \Omega\tau_d \sum_{j=1}^{m-1} \frac{B_j}{j!} \sum_{\substack{k_1+\cdots+k_j=m-1 \\ k_1\geqslant 1,\ldots,k_j\geqslant 1}} \\ \times \int_{-T/\tau_d}^{t/\tau_d} du\, \mathrm{ad}_{-iA_I^{(k_1)}(u)} \cdots \mathrm{ad}_{-iA_I^{(k_j)}(u)} \tilde{H}_I(u).\end{aligned} \tag{B3}$$

B_j for a nonnegative integer j is the Bernoulli number [55,56] and $\mathrm{ad}_X Y \equiv [X, Y]$ for given operators X and Y. For example, the second Magnus term is given by

$$A_I^{(2)}(t) = \Omega\tau_d\left(-\frac{1}{2}\right)\int_{-T/\tau_d}^{t/\tau_d} du\,\big[-iA_I^{(1)}(u), \tilde{H}_I(u)\big],$$

with $B_1 = -1/2$.

From Eq. (B3), let us show

$$\begin{aligned}A_I^{(m)}(t) &\equiv (\Omega\tau_d)^m \tilde{A}_I^{(m)}(t) \\ &= \mathcal{O}[(\Omega\tau_d)^m]\end{aligned} \tag{B4}$$

for all $m \geqslant 1$, by an induction. This implies $\tilde{A}_I^{(m)}(t) = \mathcal{O}[(\Omega\tau_d)^0]$ for all m. Equation (B4) holds for $m = 1$, which follows from Eqs. (B1) and (B2). For any $m > 1$, if Eq. (B4) holds for all k such that $1 \leqslant k < m$, we set $A_I^{(k)}(t) \equiv (\Omega\tau_d)^k \tilde{A}_I^{(k)}(t)$ and use $\mathrm{ad}_{cX} Y = c\,\mathrm{ad}_X Y$ for $c \in \mathbb{C}$ to show that Eq. (B3) is proportional to $(\Omega\tau_d)^m$. This concludes the induction for Eq. (B4) to hold for all $m \geqslant 1$.

We then proceed to show

$$\tilde{A}_I^{(m)}(t) = \mathcal{O}[(\sqrt{n})^m], \tag{B5}$$

for all $m \geqslant 1$, where n is the number of excitations in the state of the system. When the state is in a superposition of states with different numbers of excitations, n may be set to the average number of excitations. Each $\sqrt{n}$ comes from a or $a^\dagger$. Equation (B5) holds for $m = 1$, which follows from Eq. (B2) and the fact that $\tilde{H}_I(u)$ is linear in a and $a^\dagger$ in its leading order, as can be seen from Eqs. (28) and (6). Showing Eq. (B5) for any $m > 1$ can be done by another induction in the same manner as we did for deriving Eq. (B4).

Combining Eq. (B4) with Eq. (B5), we obtain Eq. (34). Similarly, Eq. (50) can be derived by substituting $A_I^{(k)}(t)$ and $\tilde{H}_I(u)$ in Eq. (B3) for $A_{II}^{\prime(k)}(t)$ and $\tilde{H}_{II}^{\prime}(t)$, respectively, for all k such that $1 \leqslant k \leqslant m$.

[1] J. I. Cirac and P. Zoller, Quantum computations with cold trapped ions, Phys. Rev. Lett. **74**, 4091 (1995).

[2] Q. A. Turchette, C. S. Wood, B. E. King, C. J. Myatt, D. Leibfried, W. M. Itano, C. Monroe, and D. J. Wineland,

Deterministic entanglement of two trapped ions, Phys. Rev. Lett. **81**, 3631 (1998).
[3] H. Levine, A. Keesling, G. Semeghini, A. Omran, T. T. Wang, S. Ebadi, H. Bernien, M. Greiner, V. Vuletić, H. Pichler, and M. D. Lukin, Parallel implementation of high-fidelity multiqubit gates with neutral atoms, Phys. Rev. Lett. **123**, 170503 (2019).
[4] C. Fang, Y. Wang, K. Sun, and J. Kim, Realization of scalable Cirac-Zoller multi-qubit gates, arXiv:2301.07564
[5] E. Hagley, X. Maître, G. Nogues, C. Wunderlich, M. Brune, J. M. Raimond, and S. Haroche, Generation of Einstein-Podolsky-Rosen pairs of atoms, Phys. Rev. Lett. **79**, 1 (1997).
[6] H.-J. Briegel, W. Dür, J. I. Cirac, and P. Zoller, Quantum repeaters: The role of imperfect local operations in quantum communication, Phys. Rev. Lett. **81**, 5932 (1998).
[7] V. Krutyanskiy, M. Canteri, M. Meraner, J. Bate, V. Krcmarsky, J. Schupp, N. Sangouard, and B. P. Lanyon, Telecom-wavelength quantum repeater node based on a trapped-ion processor, Phys. Rev. Lett. **130**, 213601 (2023).
[8] T. E. Tessier, I. H. Deutsch, A. Delgado, and I. Fuentes-Guridi, Entanglement sharing in the two-atom Tavis-Cummings model, Phys. Rev. A **68**, 062316 (2003).
[9] J.-F. Cai, X.-W. Wang, and J. Zou, Entanglement of two atoms induced by a Fock state of radiation field, Commun. Theor. Phys. **45**, 421 (2006).
[10] W. Cheng and J. Gea-Banacloche, Applications of the Hillery-Zubairy entanglement criteria to N-qubit systems: The Tavis-Cummings model, Phys. Rev. A **106**, 042425 (2022).
[11] M. S. Kim, J. Lee, D. Ahn, and P. L. Knight, Entanglement induced by a single-mode heat environment, Phys. Rev. A **65**, 040101(R) (2002).
[12] Z. Jian, S. Bin, and L. Qian-Shu, Entanglement of two superconducting charge qubits induced by quantized radiation field, Commun. Theor. Phys. **41**, 953 (2004).
[13] C. E. A. Jarvis, D. A. Rodrigues, B. L. Györffy, T. P. Spiller, A. J. Short, and J. F. Annett, Dynamics of entanglement and 'attractor' states in the Tavis-Cummings model, New J. Phys. **11**, 103047 (2009).
[14] S. S. Mirkhalaf and A. Smerzi, Entanglement detection in a coupled atom-field system via quantum Fisher information, Phys. Rev. A **95**, 022302 (2017).
[15] J. Zou, J.-F. Cai, B. Shao, and Q.-S. Li, Generation of entanglement between two noninteracting qubits via interaction with nonclassical radiation field, Commun. Theor. Phys. **44**, 259 (2005).
[16] M. Orszag and M. Hernandez, Coherence and entanglement in a two-qubit system, Adv. Opt. Photon. **2**, 229 (2010).
[17] S.-B. Zheng and G.-C. Guo, Efficient scheme for two-atom entanglement and quantum information processing in cavity QED, Phys. Rev. Lett. **85**, 2392 (2000).
[18] S. Osnaghi, P. Bertet, A. Auffeves, P. Maioli, M. Brune, J. M. Raimond, and S. Haroche, Coherent control of an atomic collision in a cavity, Phys. Rev. Lett. **87**, 037902 (2001).
[19] G.-P. Guo, C.-F. Li, J. Li, and G.-C. Guo, Scheme for the preparation of multiparticle entanglement in cavity QED, Phys. Rev. A **65**, 042102 (2002).
[20] R. E. Evans, M. K. Bhaskar, D. D. Sukachev, C. T. Nguyen, A. Sipahigil, M. J. Burek, B. Machielse, G. H. Zhang, A. S. Zibrov, E. Bielejec, H. Park, M. Lončar, and M. D. Lukin, Photon-mediated interactions between quantum emitters in a diamond nanocavity, Science **362**, 662 (2018).
[21] L. Garziano, V. Macrì, R. Stassi, O. Di Stefano, F. Nori, and S. Savasta, One photon can simultaneously excite two or more atoms, Phys. Rev. Lett. **117**, 043601 (2016).
[22] J. I. Cirac, P. Zoller, H. J. Kimble, and H. Mabuchi, Quantum state transfer and entanglement distribution among distant nodes in a quantum network, Phys. Rev. Lett. **78**, 3221 (1997).
[23] A. Reiserer and G. Rempe, Cavity-based quantum networks with single atoms and optical photons, Rev. Mod. Phys. **87**, 1379 (2015).
[24] M. Tavis and F. W. Cummings, Exact solution for an N-molecule–radiation-field Hamiltonian, Phys. Rev. **170**, 379 (1968).
[25] S. A. Hill and W. K. Wootters, Entanglement of a pair of quantum bits, Phys. Rev. Lett. **78**, 5022 (1997).
[26] W. K. Wootters, Entanglement of formation of an arbitrary state of two qubits, Phys. Rev. Lett. **80**, 2245 (1998).
[27] P. Alsing and H. J. Carmichael, Spontaneous dressed-state polarization of a coupled atom and cavity mode, Quantum Opt. **3**, 13 (1991).
[28] P. Alsing, D.-S. Guo, and H. J. Carmichael, Dynamic Stark effect for the Jaynes-Cummings system, Phys. Rev. A **45**, 5135 (1992).
[29] O. V. Zhirov and D. L. Shepelyansky, Synchronization and bistability of a qubit coupled to a driven dissipative oscillator, Phys. Rev. Lett. **100**, 014101 (2008).
[30] L. Ermann, G. G. Carlo, A. D. Chepelianskii, and D. L. Shepelyansky, Jaynes-Cummings model under monochromatic driving, Phys. Rev. A **102**, 033729 (2020).
[31] A. Faraon, I. Fushman, D. Englund, N. Stoltz, P. Petroff, and J. Vučković, Coherent generation of non-classical light on a chip via photon-induced tunnelling and blockade, Nat. Phys. **4**, 859 (2008).
[32] M. Feng, Y. P. Zhong, T. Liu, L. L. Yan, W. L. Yang, J. Twamley, and H. Wang, Exploring the quantum critical behaviour in a driven Tavis-Cummings circuit, Nat. Commun. **6**, 7111 (2015).
[33] K. Kakuyanagi, Y. Matsuzaki, C. Déprez, H. Toida, K. Semba, H. Yamaguchi, W. J. Munro, and S. Saito, Observation of collective coupling between an engineered ensemble of macroscopic artificial atoms and a superconducting resonator, Phys. Rev. Lett. **117**, 210503 (2016).
[34] S. Haroche and J.-M. Raimond, *Exploring the Quantum: Atoms, Cavities, and Photons* (Oxford University Press, Oxford, UK, 2006).
[35] C. H. Bennett, H. J. Bernstein, S. Popescu, and B. Schumacher, Concentrating partial entanglement by local operations, Phys. Rev. A **53**, 2046 (1996).
[36] C. H. Bennett, D. P. DiVincenzo, J. A. Smolin, and W. K. Wootters, Mixed-state entanglement and quantum error correction, Phys. Rev. A **54**, 3824 (1996).
[37] J. H. Eberly, N. B. Narozhny, and J. J. Sanchez-Mondragon, Periodic spontaneous collapse and revival in a simple quantum model, Phys. Rev. Lett. **44**, 1323 (1980).
[38] J. Gea-Banacloche, Collapse and revival of the state vector in the Jaynes-Cummings model: An example of state preparation by a quantum apparatus, Phys. Rev. Lett. **65**, 3385 (1990).
[39] J. E. Campbell, On a law of combination of operators bearing on the theory of continuous transformation groups, Proc. London Math. Soc. **s1-28**, 381 (1896).

[40] W. Magnus, On the exponential solution of differential equations for a linear operator, Commun. Pure Appl. Math. **7**, 649 (1954).

[41] S. Blanes, F. Casas, J. Oteo, and J. Ros, The Magnus expansion and some of its applications, Phys. Rep. **470**, 151 (2009).

[42] F. Casas, Sufficient conditions for the convergence of the Magnus expansion, J. Phys. A: Math. Theor. **40**, 15001 (2007).

[43] A. S. Moskalenko, Z.-G. Zhu, and J. Berakdar, Charge and spin dynamics driven by ultrashort extreme broadband pulses: A theory perspective, Phys. Rep. **672**, 1 (2017).

[44] R. P. Feynman, An operator calculus having applications in quantum electrodynamics, Phys. Rev. **84**, 108 (1951).

[45] A. de Oliveira Junior, M. Perarnau-Llobet, N. Brunner, and P. Lipka-Bartosik, Quantum catalysis in cavity QED, arXiv:2305.19324.

[46] G. Milburn and P. Alsing, Quantum phase transitions in a linear ion trap, in *Directions in Quantum Optics*, edited by H. J. Carmichael, R. J. Glauber, and M. O. Scully (Springer, Berlin, 2001), pp. 303–312.

[47] N. Meher and S. Sivakumar, A review on quantum information processing in cavities, Eur. Phys. J. Plus **137**, 985 (2022).

[48] S. Xie and J. H. Eberly, Triangle measure of tripartite entanglement, Phys. Rev. Lett. **127**, 040403 (2021).

[49] S. Xie, Y.-Y. Zhao, C. Zhang, Y.-F. Huang, C.-F. Li, G.-C. Guo, and J. H. Eberly, Experimental examination of entanglement estimates, Phys. Rev. Lett. **130**, 150801 (2023).

[50] D. J. Wineland, J. J. Bollinger, W. M. Itano, F. L. Moore, and D. J. Heinzen, Spin squeezing and reduced quantum noise in spectroscopy, Phys. Rev. A **46**, R6797(R) (1992).

[51] A. Sørensen, L.-M. Duan, J. I. Cirac, and P. Zoller, Many-particle entanglement with Bose-Einstein condensates, Nature (London) **409**, 63 (2001).

[52] L. Pezzé and A. Smerzi, Entanglement, nonlinear dynamics, and the Heisenberg limit, Phys. Rev. Lett. **102**, 100401 (2009).

[53] S. Sur and V. Subrahmanyam, Information scrambling and redistribution of quantum correlations through dynamical evolution in spin chains, Quantum Inf. Process. **21**, 301 (2022).

[54] T. K. Kvorning, L. Herviou, and J. H. Bardarson, Time-evolution of local information: Thermalization dynamics of local observables, SciPost Phys. **13**, 080 (2022).

[55] J. Bernoulli, *Ars conjectandi, opus posthumum. Accedit Tractatus de seriebus infinitis, et epistola gallicé scripta de ludo pilae reticularis* (Thurneysen Brothers, Basel, 1713), pp. 97–98.

[56] G. B. Arfken and H. J. Weber, *Mathematical Methods for Physicists*, 6th ed. (Elsevier Academic Press, New York, 2005), pp. 376–379.